NRC Research Press

REVIEW

Overview of recent advances performed in the study of atomic structures and radiative processes for the lowest ionization stages of heavy elements[1]

Pascal Quinet

Abstract: During the past 20 years, part of our work has been focused on the study of the atomic structure and the determination of radiative parameters in neutral and slightly ionized heavy atoms ($Z \geq 37$). These elements attracted little previous interest because of the complexity of their electronic structures, the poor knowledge of their spectra, and the difficulty to perform experimental measurements. They present, however, great interest in the development of other scientific areas, such as astrophysics and plasma physics. In this paper, we give an overview of the recent progress performed by the group of Atomic Physics and Astrophysics at Mons University (Belgium) in the theoretical modelling and the experimental analysis of such heavy elements. We also discuss some applications of the atomic data obtained in our work for the interpretation of the spectra observed from astrophysical and laboratory plasmas.

Key words: atomic data, oscillator strengths, radiative transition probabilities, heavy elements.

Résumé : Durant les 20 dernières années, une partie de notre travail a été focalisée sur l'étude de la structure atomique et la détermination des paramètres radiatifs dans les atomes lourds neutres et faiblement ionisés ($Z \geq 37$). Ces éléments avaient attiré peu d'intérêt auparavant à cause de la complexité de leurs structures électroniques, du manque de connaissance de leurs spectres et de la difficulté à réaliser des mesures expérimentales. Ils présentent cependant un grand intérêt pour le développement d'autres domaines scientifiques comme l'astrophysique et la physique des plasmas. Dans cet article, nous présentons un aperçu général des progrès récents réalisés par le groupe de Physique Atomique et Astrophysique de l'Université de Mons (Belgique) dans la modélisation et l'analyse expérimentale de tels éléments lourds. Nous discutons également quelques applications des données atomiques obtenues dans notre travail pour l'interprétation des spectres observés à partir de plasmas astrophysiques et de laboratoire.

Mots-clés : ions lourds, données atomiques, temps de vie radiatifs, forces d'oscillateur, probabilités de transition.

1. Introduction

Over the past 20 years, our group of Atomic Physics and Astrophysics at the University of Mons, Belgium, has been involved in large-scale determination of radiative parameters in neutral to moderately ionized heavy atoms, ranging typically from rubidium ($Z = 37$) to americium ($Z = 95$). These species formerly attracted much less interest than lighter elements, essentially due to the complexity of their atomic structures, to the poor knowledge of their spectra, and to the difficulty of performing experimental measurements. Many of these heavy elements, however, play a key role in other scientific fields, such as astrophysics, plasma physics, laser physics, photonics, material science, etc.

In astrophysics, a current problem in stellar nucleosynthesis consists of clarifying the respective importance of rapid- (r) and slow- (s) neutron capture processes for the buildup of heavy elements in the Galaxy (see e.g., refs. 1, 2). A detailed investigation of such processes is not possible without a great deal of accurate atomic data, not only for the prominent stellar lines but also for a huge number of weak absorption features, which are now commonly observable on high resolution astrophysical spectra. Moreover, some heavy elements have been detected in chemically peculiar stars with overabundances sometimes several orders of magnitude higher than the solar values (see e.g., refs. 3–5). In this context, the determination of radiative parameters characterizing the first ionization stages of heavy atoms (including the lanthanides and some actinides) is of course vital, not only for deriving stellar chemical compositions, but also for understanding the large overabundances that are related to diffusion processes and magnetic field effects.

In laboratory plasma physics, an element like tungsten is important for thermonuclear fusion research because it is used as a plasma facing material in tokamak devices. Due to its high melting point and thermal conductivity, and its low tritium retention and erosion rate under plasma loading, tungsten is indeed a very attractive element for tokamaks. The International Thermonuclear Experimental Reactor (ITER), which will be the next step toward the realization of fusion, will use tungsten, together with beryllium and carbon-fiber reinforced composites, as plasma-facing materials [6–10]. Atomic data for all ionization stages of tungsten are therefore urgently needed. Some other heavy elements present also a particular interest in fusion research. This is, for example, the case for molybdenum, which is used as compo-

Received 12 October 2016. Accepted 17 December 2016.

P. Quinet. Physique Atomique et Astrophysique, Université de Mons, B-7000 Mons, Belgium; IPNAS, Université de Liège, B-4000 Liège, Belgium.
Email for correspondence: Pascal.Quinet@umons.ac.be.

[1]This paper is part of a Special Issue on the 12th International Colloquium on Atomic Spectra and Oscillator Strengths for Astrophysical and Laboratory Plasmas held at the Universidade de São Paulo on 4–7 July, 2016.

nent of plasma-facing material in different devices, such as Alcator C-Mod reactor [11] or the experimental advanced superconducting tokamak, EAST [12].

It is also well known that triply ionized lanthanides play an important role in different areas, such as laser physics, lighting industry, photonics, molecular biology, medical diagnostics, etc. (see e.g., refs. 13–16). Because of their unique photophysical properties, in particular with respect to the generation and amplification of light, the luminescence of these ions in compounds has been widely studied. This luminescence is the result of the competition of radiative and non-radiative relaxation processes of electronically excited states in lanthanide ions that are characterized by a multitude of energy levels particularly because of the unfilled 4f orbital. Understanding the light emission from triply ionized lanthanides therefore requires reliable information about their atomic structure and radiative parameters.

Because of the difficulty of obtaining large sets of experimental data for many atoms or ions, the theoretical approaches cannot be ignored. Their limitations, however, arise from the importance of strong electronic correlation effects, including both intravalence and core–valence interactions, and from the presence of significant relativistic effects. During recent years, systematic calculations mainly based on pseudo-relativistic Hartree–Fock (HFR) and fully relativistic multiconfiguration Dirac–Fock methods have appeared extremely useful and successful for providing a large set of new radiative parameters for the first ionization stages of heavy atoms. In most cases, their accuracy was assessed through detailed comparisons with laboratory data measured in the framework of different experimental techniques, such as the time-resolved laser-induced fluorescence method, the laser-induced breakdown spectroscopy, the beam–foil spectroscopy and the heavy ion storage ring device.

In the present paper, we give an overview of the recent advances performed by the Atomic Physics and Astrophysics group at Mons University concerning the experimental and (or) theoretical determination of radiative properties (oscillator strengths, transition probabilities, branching fractions, radiative lifetimes, etc.) of neutral through moderately ionized atoms, from rubidium up to americium. This represents an update and an extension of recent reviews on similar topics [17–20], which were limited to studies published in 2011 or earlier.

2. Theoretical calculations

For the lowest ionization stages of heavy elements, the choice of a theoretical method for modeling the electronic structure and computing the radiative rates is rather difficult. Configuration interaction and relativistic effects are expected to be important in such atomic systems. In our work, we used pseudo-relativistic (based on the Schrödinger equation) and purely relativistic (based on the Dirac equation) methods, the former approach appearing, however, in general better adapted to large-scale calculations and less subject to convergence problems than the latter one, in particular for neutral and singly ionized atoms.

2.1. HFR method including core-polarization

In the HFR method [21], a set of orbitals are obtained for each electronic configuration by solving the Hartree–Fock equations for the spherically averaged atom. The equations are the result of the application of the variational principle to the configuration average energy. Relativistic corrections are also included in this set of equations (i.e., the Blume–Watson spin–orbit, mass variation, and one-body Darwin terms). The Blume–Watson spin–orbit term comprises the part of the Breit interaction that can be reduced to a one-body operator. The multiconfiguration Hamiltonian matrix is constructed and diagonalized in the *LSJ* representation within the framework of the Slater–Condon theory. Each matrix element is a sum of products of Racah angular coefficients and radial integrals, that is,

$$H_{ab} = \sum_j c_{abj} I_{abj} \tag{1}$$

The radial parameters, I_{abj}, correspond to the configuration average energies (E_{av}), the monoconfiguration (F^k, G^k) and configuration interaction (R^k) Slater integrals, the spin–orbit parameters (ζ_{nl}) and, if needed, the effective interaction parameters (α, β, γ) [21]. These parameters can be adjusted to fit the available experimental energy levels in a least-squares approach. This approach, however, is strongly dependent upon the quantity and the quality of the observed energy levels. The eigenvalues and the eigenstates obtained in this way (ab initio or semi-empirically) are used to compute the wavelengths, the transition probabilities, and the oscillator strengths for all possible transitions.

For slightly ionized heavy atoms, accurate calculations of atomic structure should allow for both intravalence and core–valence correlation. In complex polyelectronic atomic systems, this can produce a very large number of states to deal with in the computations. As an example, the consideration of the $6p^4$–$6p^3 6d$ transition array in polonium (Z = 84) with intravalence interactions up to n = 6, l = 3 outside the $[Xe]4f^{14}5d^{10}6s^2$ closed subshells gives rise to 196 even- and 594 odd-parity levels while a model including core–valence correlations by means of single excitations from 4f, 5d, and 6s core subshells leads to 10 596 and 10 910 energy levels in each parity, respectively. It is clear that this number can very rapidly increase if we want to consider several types of transitions with higher values of the n and l quantum numbers. In our work, within the framework of the HFR method, we used an approach in which the largest part of the intravalence correlation is represented within a configuration interaction scheme, that is, by explicitly including a set of electronic configurations in the physical model, while core–valence correlation is approximated by a core-polarization (CPOL) model potential. As suggested by Migdalek and Baylis [22], for atomic systems with n valence electrons, the one-particle operator of this potential can be written as

$$V_{P1} = -\frac{1}{2}\alpha_d \sum_{i=1}^{n} \frac{r_i^2}{\left(r_i^2 + r_c^2\right)^3} \tag{2}$$

where α_d is the dipole polarizability of the ionic core, for which numerical values can be found in the literature (see e.g., refs. 23, 24), and r_c is the cutoff radius that is arbitrarily chosen as a measure of the size of the ionic core. In practice, this latter parameter is usually chosen to be equal to the HFR mean value $\langle r \rangle$ for the outermost ionic core orbital.

In addition, the interaction between the modified electric fields experienced by the valence electrons gives rise to a two-particle contribution given by

$$V_{P2} = -\alpha_d \sum_{i>j} \frac{\boldsymbol{r}_i \cdot \boldsymbol{r}_j}{\left[\left(r_i^2 + r_c^2\right)\left(r_j^2 + r_c^2\right)\right]^{3/2}} \tag{3}$$

To allow for a more accurate treatment of core–valence interactions, we added a further correction to take the penetration of the core by the valence electrons into account. Following the formalism developed by Hameed and coworkers [25, 26], this effect can be modelled by the addition to the radial integral

$$\int_0^\infty P_{nl}(r) \frac{r}{\left(r^2 + r_c^2\right)^{3/2}} P_{n'l'}(r) dr \tag{4}$$

Table 1. Comparison of computed and experimental lifetimes (in ns) for the [Xe]6p $^2P_{1/2,3/2}$ levels in La III and the [Xe]4f^{14}6p $^2P_{1/2,3/2}$ levels in Lu III.

	Lifetime (ns)	
Method	6p $^2P_{1/2}$	6p $^2P_{3/2}$
La III		
HF	1.64	1.39
HFR	1.53	1.28
HFR+CPOL	1.88	1.56
HFR+CPOL+CPEN	1.86	1.54
Experiment[a]	1.95±0.20	1.56±0.20
Lu III		
HF	1.49	1.00
HFR	1.57	1.06
HFR+CPOL	2.03	1.38
HFR+CPOL+CPEN	2.23	1.47
Experiment[a]	2.20±0.20	1.55±0.20

[a]From TR-LIF measurements [126].

appearing in (2) of the core-penetration (CPEN) term

$$\frac{1}{r_c^3}\int_0^{r_c} P_{nl}(r) r P_{n'l'}(r) dr \tag{5}$$

When including the CPOL and CPEN corrections in the Hamiltonian, the dipole-moment operator in the transition matrix element has also to be modified for consistency. More precisely, the dipole radial integral

$$\int_0^{\infty} P_{nl}(r) r P_{n'l'}(r) dr \tag{6}$$

has to be replaced by

$$\int_0^{\infty} P_{nl}(r) r \left[1 - \frac{\alpha_d}{\left(r^2 + r_c^2\right)^{3/2}}\right] P_{n'l'}(r) dr - \frac{\alpha_d}{r_c^3}\int_0^{r_E} P_{nl}(r) r P_{n'l'}(r) dr \tag{7}$$

The HFR method, modified in that way, has been successful for predicting radiative parameters in many different situations. In Table 1, we illustrate the cases of La III and Lu III by showing the convergence of the radiative lifetimes computed using different levels of approximation to the experimental values. It is clear that CPOL and CPEN effects appear to play a significant role, at least as important as relativistic contributions. Moreover, it has been demonstrated in many situations that the HFR approach gives rise to similar results to those obtained with purely relativistic methods, provided configuration interaction is considered in the calculations in a sufficiently extensive way. This is illustrated in Table 2 where oscillator strengths computed using the HFR + CPOL + CPEN and multiconfigurational Dirac–Fock (MCDF, see Section 2.3) methods are compared for 5s^2 $^1S_0$–5s5p $^{1,3}P_1$ transitions along the cadmium isoelectronic sequence.

2.2. Oscillator strength parameterization (OSP) approach

In some specific ions, we have compared the results obtained with the HFR + CPOL + CPEN method with transition rates computed with another semi-empirical approach based on the parametrization of oscillator strengths. The complete details of this method were described for the first time in a paper presented by Ruczkowski et al. [27] and we therefore only give a brief summary here.

Table 2. Comparison of HFR+CPOL+CPEN and MCDF oscillator strengths of 5s^2 $^1S_0$–5s5p $^{1,3}P_1$ transitions along the cadmium isoelectronic sequence.

			MCDF[a]	
Z	Ion	HFR+CPOL+CPEN[a]	Babushkin	Coulomb
5s^2 $^1S_0$–5s5p $^1P_1$				
48	Cd I	1.388	1.455	1.401
49	In II	1.522	1.562	1.538
50	Sn III	1.540	1.567	1.561
51	Sb IV	1.534	1.557	1.560
52	Te V	1.528	1.541	1.551
53	I VI	1.514	1.523	1.538
54	Xe VII	1.511	1.503	1.523
55	Cs VIII	1.501	1.482	1.504
56	Ba IX	1.496	1.461	1.486
57	La X	1.496	1.440	1.467
5s^2 $^1S_0$–5s5p $^3P_1$				
48	Cd I	0.002	0.002	0.002
49	In II	0.005	0.005	0.005
50	Sn III	0.009	0.009	0.010
51	Sb IV	0.014	0.014	0.016
52	Te V	0.020	0.021	0.022
53	I VI	0.026	0.028	0.030
54	Xe VII	0.034	0.035	0.039
55	Cs VIII	0.042	0.044	0.047
56	Ba IX	0.051	0.052	0.057
57	La X	0.060	0.064	0.064

[a]The details of calculations are given in ref. 62.

For an electric dipole transition, the weighted oscillator strength gf is related to the line strength S [21]

$$gf = 8\pi^2 mca_0^2 \frac{\sigma}{3h} S = 303.76 \times 10^{-8} \sigma S \tag{8}$$

where a_0 is the Bohr radius, $\sigma = |E(\gamma J) - E(\gamma' J')|/hc$, h is Planck's constant while $E(\gamma J)$ and $E(\gamma' J')$ are the energies of the initial and final states, respectively. The electric dipole line strength is defined by

$$S = |\langle \gamma J || \mathbf{P^1} || \gamma' J' \rangle|^2 \tag{9}$$

The tensorial operator $\mathbf{P^1}$ in the reduced matrix element represents the electric dipole moment.

For multiconfiguration systems, the wavefunctions $|\gamma J\rangle$ and $|\gamma' J'\rangle$ are expanded in terms of a set of basis functions $|\alpha\, LSJ\rangle$ and $|\alpha' L' S' J'\rangle$, respectively,

$$|\gamma J\rangle = \sum_i c_i |\alpha LSJ\rangle \qquad |\gamma' J'\rangle = \sum_j c'_j |\alpha' L' S' J'\rangle \tag{10}$$

The square root of the line strength may be written in the following form

$$S^{1/2}_{\gamma\gamma'} = \sum_i \sum_j c_i c'_j \langle \alpha LSJ || \mathbf{P^1} || \alpha' L' S' J' \rangle \tag{11}$$

From (8) and (11), we can express the gf-value as

$$(gf)^{1/2} = (303.76\sigma \times 10^{-8})^{1/2} \sum_i \sum_j c_i c'_j \langle \alpha LSJ || \mathbf{P^1} || \alpha' L' S' J' \rangle \tag{12}$$

In the OSP method, the angular part of the electric dipole moment appearing in (12) is computed with the help of the Racah algebra and the level eigenvectors, as obtained with Cowan's code [21], while the radial integrals, that is,

$$\int_0^\infty R_{nl}(r) r R_{n'l'}(r) dr \tag{13}$$

are treated as free parameters in a least-squares fit to available experimental oscillator strengths.

2.3. Purely relativistic MCDF method

Finally, the entirely relativistic MCDF method [28–30] implemented in the latest versions of the General Relativistic Atomic Structure Program (GRASP) [31–33] was also used to model the atomic structure and compute the radiative parameters in several cases. In this approach, the Hamiltonian is given by

$$H = \sum_{i=1}^{N} \left[c\alpha_i \cdot p_i + (\beta_i - 1)c^2 - \frac{Z}{r_i} \right] + \sum_{i<j}^{N} \frac{1}{r_{ij}} \tag{14}$$

where c is the speed of light and α and β are the Dirac matrices. For each parity, the atomic state functions are given as an expansion over *jj*-coupled configuration state functions

$$|\gamma J M_J\rangle = \sum_i c_i |\alpha_i J M_J\rangle \tag{15}$$

The configuration state functions are in turn built from Slater determinants constructed on the four-component Dirac orbitals

$$\varphi_{n\kappa m}(r, \theta, \phi) = \frac{1}{r} \begin{bmatrix} P_{n\kappa}(r)\chi_{\kappa m}(\theta, \phi) \\ iQ_{n\kappa}(r)\chi_{-\kappa m}(\theta, \phi) \end{bmatrix} \tag{16}$$

where $P_{n\kappa}(r)$ and $Q_{n\kappa}(r)$ are the large and small component radial wavefunctions, respectively, and $\chi_{\kappa m}(\theta, \phi)$ is the spinor spherical harmonic in the *lsj* coupling scheme. The relativistic angular quantum number κ is given by

$$\kappa = \pm\left(j + \frac{1}{2}\right) \tag{17}$$

where j is the quantum number associated with the total kinetic moment of the electron, the sign before the parenthesis corresponding to the coupling relation between the electron orbital momentum, l, and its spin (i.e., $l = j \pm 1/2$).

The relativistic two-body Breit interaction and the quantum electrodynamic corrections due to self-energy and vacuum polarization [29] were also considered in the computations. In the MCDF variational procedure, the radial functions and the expansion coefficients c_i are optimized to self-consistency. This can be done using different schemes. In the optimal level option, only the energy of an individual level $|\gamma J\rangle$ is minimized while in the extended optimal level scheme, the minimization is extended over several selected levels. The third option is the average level scheme where spin–orbitals are chosen to minimize the average energy of configuration state functions with different total angular momentum J. Finally, in the fourth option, extended average level, averaging of the energy expression is extended to all configuration functions, usually employing statistical weights $(2J + 1)$ as weighting factors.

3. Experimental measurements

Calculations of atomic structures and transition rates in heavy ions like those considered in our work can be extremely complex and need to be tested by comparisons with laboratory measurements to deduce relevant information concerning their predictive power. Consequently, to assess the accuracy of our theoretical models, we also carried out a large number of experimental studies using different spectroscopy techniques chosen according to the atomic system or radiative process of interest.

3.1. Time-resolved laser-induced fluorescence

For a large number of ions considered in our different investigations, atomic lifetime measurements were performed by means of time-resolved laser-induced-fluorescence spectroscopy using the experimental setups installed at the Lund Laser Centre, Sweden, and at the Jilin University, China. A few measurements were also carried out in collaboration with the University of Wisconsin in Madison, USA. The time-resolved laser-induced-fluorescence technique is interesting because the selective excitation does allow avoidance of eventual cascading problems. In addition, many levels are accessible through the use of different excitation schemes, such as one-step, two-step or two-photon excitation, and different laser dyes. Different ionization stages can be investigated using laser-produced plasmas, from neutral to doubly- or even trebly-ionized atoms and a wide range of lifetime values are accessible, typically from 1 ns to several hundreds of nanoseconds, with an accuracy of a few percent in most cases. In this technique, described, for example, in refs. 17, 34, free atoms and ions are produced in a plasma zone by laser ablation. A metallic foil, rotating in a vacuum chamber, is irradiated perpendicularly by a laser pulse of a few nanoseconds' duration. When the laser-produced plasma is expanded about a few millimetres above the target, it is crossed by an excitation laser beam. The fluorescence generated is collected by a fused-silica lens, and then appropriately filtered by a monochromator, to be finally detected by a microchannel-plate photomultiplier tube. The decay curves are analyzed and the lifetimes are extracted by a least-squares fit of a single exponential decay, convoluted to the data by the measured laser pulse, if necessary.

3.2. Laser-induced breakdown spectroscopy

In a few cases, branching fractions have been measured, in collaboration with colleagues from the Complutense University of Madrid, Spain, by means of the laser-induced breakdown spectroscopy. The experimental details are presented in the corresponding papers (see e.g., ref. 35), therefore only a brief description is given here. In this technique, free atoms and ions were produced by laser ablation using a Nd:YAG laser at 1064 nm wavelength with 7 ns pulse duration at 20 Hz and 160 mJ pulse energy. The plasma was generated by focusing the laser beam on the surface of a rotating target placed in a vacuum chamber. The light emission from the plasma was directed on to the entrance slit of a 1 m grating Czerny–Turner monochromator with 2 400 grooves/mm and 0.03 nm resolution. The spectra were registered by a time-resolved optical multichannel analyzer system, allowing the recording of 10 nm spectrum sections. The best signal-to-noise ratio was retained by using different delay times following the laser pulse and by choosing the optimal value of this delay. The experiments were carried out with a glass filter placed in front of the entrance slit of the monochromator to avoid the possible influence of the second-order spectra. The spectral lines were analyzed with a special software allowing us to deduce the intensities, the full widths at half maximum (FWHM) as well as the Gaussian and Lorentzian components of the profiles. With this program, it was also possible to calibrate the spectra, to subtract the background, and to separate overlapping or closely spaced lines. The intensities were then averaged from generally about ten measurements to determine the final values of all observed spectral lines.

3.3. Beam–foil spectroscopy

The beam–foil spectroscopy represents one of the rare methods allowing the investigation of the atomic structure and the measurement of radiative lifetimes in moderately charged ions. This experimental technique was used in a few cases in our work (i.e., for Xe VI–IX and La IV ions) [36–39]. The instrumental device of Liège University, Belgium, was employed for that purpose. The experimental details can be found in the relevant publications and, consequently, we just recall here the main characteristics of this method. An ion beam was produced by a Van de Graaff accelerator equipped with a conventional radio-frequency source. The beam was analyzed by a magnet and focused inside a target chamber. Beams with energies up to 2 MeV could be produced. Inside the chamber, the beam was excited and ionized by passing through a very thin (about 20 μg/cm^2) carbon foil. Just after the foil, the light, emitted by the excited ions, was observed at right angle by a Seya-Namioka-type spectrometer equipped with an R = 1 m concave 1200 l/inch grating blazed for normal incidence at 110.0 nm. The entrance slit of the spectrometer had a width of 120 μm and was situated at 15 mm from the axis of the 10 mm diameter ion beam. The light was detected by a thin, back-illuminated, liquid nitrogen cooled charge-coupled device (CCD) detector specially developed for far ultraviolet measurements. The CCD worked under vacuum and was cooled down by liquid nitrogen to –90 °C for noise reduction. The CCD, which replaces the exit slit of the spectrometer, was tilted to an angle of 125° relative to the spectrometer exit arm axis to be tangential to the Rowland circle. Under that geometry, it has a dispersion of 0.02 nm/pixel and detects light over a 20 nm wide region with a fairly constant resolution giving a line width (FWHM) of about 0.12 nm. The whole system was working under vacuum (10^{-5} Torr). The CCD images were transferred to a networked computer and analyzed by specially written software. A problem affecting the beam–foil spectra is the rather low spectral resolution just mentioned. At that resolution, we find many lines blended. In addition, beam–foil excitation is non-selective; this results in the production of a range of ion charge states (the spectra of neighboring ions often overlap each other) and in the excitation of a plethora of individually weak spectral lines that arise from the multitude of excited levels. The use of a CCD camera represents a major improvement over spectral scanning techniques and assures both better data accumulation (counting statistics) and constancy of conditions across a selected spectral range.

3.4. Heavy ion storage ring

For metastable states, whose lifetimes may range from milliseconds up to several years under ordinary vacuum conditions, some experimental measurements have been performed at the heavy ion storage ring CRYRING. This device was operated by the Manne Siegbahn Laboratory of Stockholm University until 2009 and has subsequently been replaced by the new setup DESIREE (double electrostatic ion ring experiment). The measurements made at CRYRING have been widely described in review papers [40, 41] and the discussion will not be repeated here. Let us just recall that this technique is suitable for the measurement of long atomic lifetimes (up to several tens of seconds) and gives access to low-lying metastable states that depopulate through forbidden transitions, such as magnetic dipole (M1), electric quadrupole (E2), magnetic quadrupole (M2), electric octupole (E3) transitions, etc. Such states are frequently important in astrophysics. They also represent an accurate test of the theoretical models because of their high sensitivity to small intermediate coupling or configuration interaction effects. The radiative lifetimes measured at CRYRING generally reached an accuracy of 1% and, in different cases, we applied a laser probing of the populations. In this latter technique, an allowed transition is induced from the metastable level to a short-lived upper level, whose lifetime is of a few nanoseconds and that decay back to the metastable or to another low-lying level, the intensity of the fluorescence decay being proportional to the population of the metastable level.

It is worth mentioning that this experimental technique allowed us to obtain very nice (sometimes unexpected) results. As an example, the determination of the radiative decay of the metastable level 5d $^4D_{7/2}$ in Xe II has appeared particularly interesting [42]. Lifetime measurements of this level in a storage ring are difficult because magnetic mixing of the metastable with a short-lived level quenches its population. Using a theoretical MCDF model, we found that the decay is heavily dominated by an M2 transition and not by M1/E2 transitions (as usually expected). Decay rates were determined at different magnetic field strengths B to allow a nonlinear extrapolation to B = 0 and the experimental measurement (τ = 2.4 ± 0.8 s) was found in agreement with the calculated MCDF value (2.32 s), but much smaller than previous estimations. Another example concerns the lifetime measurement performed for the metastable 5d $^2D_{3/2}$ level of Ba II. It turned out that the experimental result obtained in our study (τ = 89.4 ± 15.6 s) [43] was the longest radiative lifetime ever measured in a storage ring. This value was supported by new HFR calculations including a large amount of configuration interaction from which we deduced τ = 82 s.

Table 3. Ground configurations for the first three ionization stages of atoms belonging the fifth row of the periodic table.

		Ground configuration		
Z	Element	I	II	III
37	Rb	5s	4p^6	4p^5
38	Sr	5s^2	5s	4p^6
39	Y	4d5s^2	5s^2	4d
40	Zr	4d^{2}5s^2	4d^{2}5s	4d^2
41	Nb	4d^{4}5s	4d^4	4d^3
42	Mo	4d^{5}5s	4d^5	4d^4
43	Tc	4d^{5}5s^2	4d^{5}5s	4d^5
44	Ru	4d^{7}5s	4d^7	4d^6
45	Rh	4d^{8}5s	4d^8	4d^7
46	Pd	4d^{10}	4d^9	4d^8
47	Ag	4d^{10}5s	4d^{10}	4d^9
48	Cd	4d^{10}5s^2	4d^{10}5s	4d^{10}
49	In	4d^{10}5s^{2}5p	4d^{10}5s^2	4d^{10}5s
50	Sn	4d^{10}5s^{2}5p^2	4d^{10}5s^{2}5p	4d^{10}5s^2
51	Sb	4d^{10}5s^{2}5p^3	4d^{10}5s^{2}5p^2	4d^{10}5s^{2}5p
52	Te	4d^{10}5s^{2}5p^4	4d^{10}5s^{2}5p^3	4d^{10}5s^{2}5p^2
53	I	4d^{10}5s^{2}5p^5	4d^{10}5s^{2}5p^4	4d^{10}5s^{2}5p^3
54	Xe	4d^{10}5s^{2}5p^6	4d^{10}5s^{2}5p^5	4d^{10}5s^{2}5p^4

4. Results obtained so far

4.1. Fifth row elements

The fifth row elements are those appearing in the periodic table between rubidium (Z = 37) and xenon (Z = 54). As a general rule, these elements fill their 5s subshell first, then their 4d, and 5p subshells, in that order; however, there are exceptions, as shown in Table 3 which lists the ground electronic configurations for the first three ionization stages of these atoms. More generally, configurations of the type 4d^k, 4d^{k-1}nl, 4d$^{k-2}nln'l'$ and 4d$^{k-3}nln'l'n''l''$ often overlap each other in these atomic systems giving rise to strong interactions between states belonging to such configurations. This is illustrated in Fig. 1 showing the overlap of the lowest odd-parity configurations in neutral niobium (Z = 41). Consequently, the calculation of electronic structure and radiative parameters for atoms and slightly charged ions belonging to the fifth row of the periodic table is a demanding and time-consuming challenge. In Table 4, we report a summary of the results we have obtained so far in these elements.

Fig. 1. Low-lying odd-parity configurations in Nb I, as computed by the HFR method.

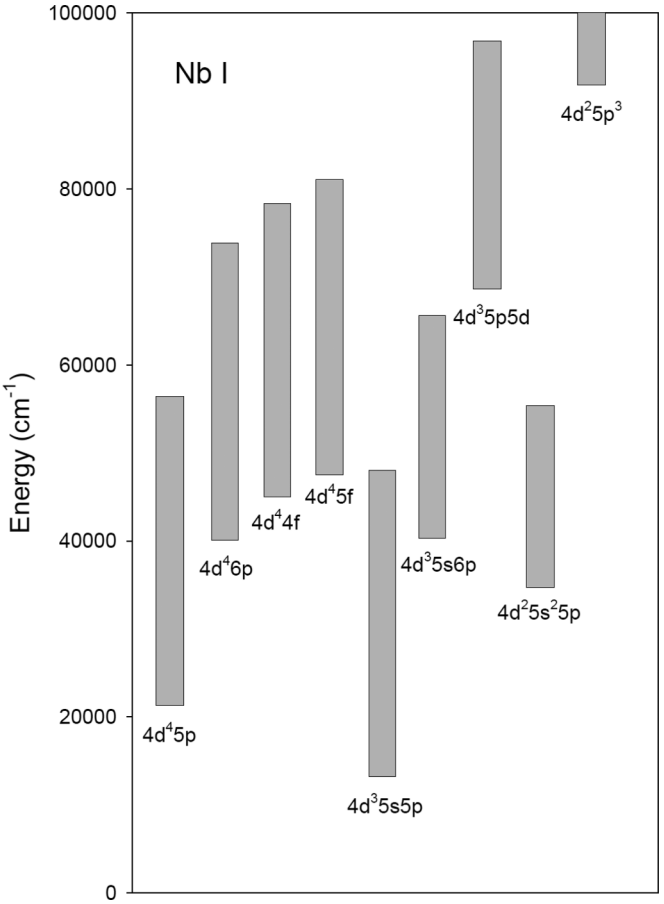

If neutral and singly ionized atoms of this group had been the subject of many of our works in the period 1996–2011, doubly ionized species still considerably suffered from the lack of accurate atomic data. During the past 5 years, we notably focused our work on the particular cases of Rb III (Z = 37), Mo III (Z = 42), Rh III (Z = 45), Pd III (Z = 46), Ag III (Z = 47), and Te III (Z = 52) for which no (or very few) radiative rates were available in the literature. For all these ions, the HFR + CPOL + CPEN method has been combined to a semi-empirical adjustment of radial parameters minimizing the differences between calculated energy levels and available experimental values to compute transition probabilities and oscillator strengths for a large number of spectral lines [69–72]. Because of the lack of radiative lifetime measurements, the quality of our calculations could only be estimated from isoelectronic comparisons, in particular from results we had formerly published in Nb II (isoelectronic of Mo III) [73], in Ru II (isoelectronic of Rh III) [74], and in Rh II (isoelectronic of Pd III) [75], for which similar HFR + CPOL + CPEN models revealed a very good agreement (generally within 10%) with accurate radiative lifetimes measured by means of the time-resolved laser-induced fluorescence technique. An accuracy of the same kind can thus be expected for the decay rates computed for the doubly charged ions considered in our new studies, at least for the most intense transitions.

Reliable radiative data in fifth row ions are particularly needed in astrophysics and, more specifically, for testing stellar nucleosynthesis models. As an example, already in 1973, Cowley et al. [76] were able to obtain abundance estimates for eight elements in the star HR 465 near the r-process peaks at tellurium and osmium. A large overabundance of tellurium was obtained by assuming that

Table 4. Experimental and theoretical methods used in our work for the determination of radiative parameters in fifth row elements (Z = 37–54) and related references.

Z	Ion	Experimental method[a]	Theoretical method[b]	References
37	Rb III	—	HFR	[69]
39	Y II	TR-LIF	HFR	[44]
	Y III	TR-LIF	HFR	[44]
40	Zr I	TR-LIF	HFR	[45]
		TR-LIF	HFR	[46]
	Zr II	TR-LIF	HFR	[47]
		—	HFR, OPS	[48]
	Zr IV	—	HFR	[181]
	Zr V	—	HFR	[181]
	Zr VI	—	HFR	[181]
	Zr VII	—	HFR	[181]
41	Nb I	TR-LIF	HFR	[49]
	Nb II	TR-LIF	HFR	[73]
	Nb III	—	HFR	[73]
42	Mo II	—	HFR	[50]
		TR-LIF	HFR	[51]
		TR-LIF	HFR	[52]
	Mo III	—	HFR	[70]
	Mo IV	—	HFR	[182]
	Mo V	—	HFR	[182]
	Mo VI	—	HFR	[182]
	Mo VII	—	HFR	[182]
43	Tc II	—	HFR	[53]
44	Ru I	TR-LIF	HFR	[54]
	Ru II	TR-LIF	HFR	[74]
	Ru III	—	HFR	[74]
45	Rh I	TR-LIF	HFR	[55]
	Rh II	TR-LIF	HFR	[75]
		TR-LIF	HFR	[56]
	Rh III	—	HFR	[71]
46	Pd I	TR-LIF	HFR	[57]
	Pd II	—	HFR	[58]
	Pd III	—	HFR	[71]
47	Ag II	LIBS	HFR	[59]
		LIBS	HFR	[60]
		LIBS	HFR	[61]
	Ag III	—	HFR	[71]
48	Cd I	—	HFR, MCDF	[62]
		TR-LIF	HFR	[63]
	Cd II	TR-LIF	HFR	[63]
49	In II	—	HFR, MCDF	[62]
50	Sn I	TR-LIF	HFR	[64]
		TR-LIF	HFR	[65]
		TR-LIF	HFR	[66]
	Sn III	—	HFR, MCDF	[62]
51	Sb I	TR-LIF	MCDF	[67]
	Sb IV	—	HFR, MCDF	[62]
52	Te II	—	HFR, MCDF	[72]
	Te III	—	HFR, MCDF	[72]
	Te V	—	HFR, MCDF	[62]
53	I VI	—	HFR, MCDF	[62]
54	Xe II	HISR	MCDF	[42]
	Xe IV	—	HFR	[181]
	Xe V	—	HFR	[181]
		—	HFR	[68]
	Xe VI	BFS	HFR	[36]
		—	HFR	[183]
	Xe VII	BFS	HFR, MCDF	[37]
		—	HFR	[181]
		—	HFR, MCDF	[62]
	Xe VIII	BFS	HFR, MCDF	[37]
	Xe IX	BFS	HFR, MCDF	[38]

[a]Experimental methods used in our work: TR-LIF, time-resolved laser-induced-fluorescence; LIBS, laser induced-breakdown spectroscopy; BFS, beam–foil spectroscopy; HISR, heavy-ion storage ring.

[b]Theoretical methods used in our work: HFR, pseudo-relativistic Hartree–Fock (including CPOL and CPEN contributions or including core–valence correlation explicitly); OPS, oscillator strength parametrization; MCDF, multiconfiguration Dirac–Fock.

Table 5. Ground configurations for the first three ionization stages of atoms belonging the sixth row of the periodic table.

		Ground configuration		
Z	Element	I	II	III
55	Cs	6s	$5p^6$	$5p^5$
56	Ba	$6s^2$	6s	$5p^6$
72	Hf	$4f^{14}5d^26s^2$	$4f^{14}5d6s^2$	$4f^{14}5d^2$
73	Ta	$4f^{14}5d^36s^2$	$4f^{14}5d^36s$	$4f^{14}5d^3$
74	W	$4f^{14}5d^46s^2$	$4f^{14}5d^46s$	$4f^{14}5d^4$
75	Re	$4f^{14}5d^56s^2$	$4f^{14}5d^56s$	$4f^{14}5d^5$
76	Os	$4f^{14}5d^66s^2$	$4f^{14}5d^66s$	$4f^{14}5d^56s$
77	Ir	$4f^{14}5d^76s^2$	$4f^{14}5d^76s$	$4f^{14}5d^7$
78	Pt	$4f^{14}5d^96s$	$4f^{14}5d^9$	$4f^{14}5d^8$
79	Au	$4f^{14}5d^{10}6s$	$4f^{14}5d^{10}$	$4f^{14}5d^9$
80	Hg	$4f^{14}5d^{10}6s^2$	$4f^{14}5d^{10}6s$	$4f^{14}5d^{10}$
81	Tl	$4f^{14}5d^{10}6s^26p$	$4f^{14}5d^{10}6s^2$	$4f^{14}5d^{10}6s$
82	Pb	$4f^{14}5d^{10}6s^26p^2$	$4f^{14}5d^{10}6s^26p$	$4f^{14}5d^{10}6s^2$
83	Bi	$4f^{14}5d^{10}6s^26p^3$	$4f^{14}5d^{10}6s^26p^2$	$4f^{14}5d^{10}6s^26p$
84	Po	$4f^{14}5d^{10}6s^26p^4$	$4f^{14}5d^{10}6s^26p^3$	$4f^{14}5d^{10}6s^26p^2$
85	At	$4f^{14}5d^{1}06s^26p^5$	$4f^{14}5d^{10}6s^26p^4$	$4f^{14}5d^{10}6s^26p^3$
86	Rn	$4f^{14}5d^{10}6s^26p^6$	$4f^{14}5d^{1}06s^26p^5$	$4f^{14}5d^{10}6s^26p^4$

the oscillator strengths were equal to log *gf* = 0.0, which was obviously a rough approximation imposed by the lack of data on oscillator strengths. More recently, neutral tellurium has been detected by Roederer et al. [77] in three metal-poor stars enriched by products of r-process nucleosynthesis using near-ultraviolet spectra obtained with the Space Telescope Imaging Spectrograph on board the Hubble Space Telescope. This element had not been detected previously in Galactic halo stars. The tellurium ions (Te II and Te III) had not been identified in stellar spectra, one of the obvious reasons being the lack of radiative rates in these two ions, the results available [78] concerning only the forbidden transitions. Another reason results from the fact that a quantitative analysis of Te II lines is complicated by hyperfine structure effects [79]. This lack of radiative data therefore justified the effort we have made in our work [72], further motivated by the recent new analysis of Te III spectrum [80]. More precisely, a first set of transition probabilities has been obtained for 439 transitions of Te II in the spectral range between 77 and 997 nm and for 284 transitions of Te III in the range 52–901 nm. Their accuracy has been assessed through the comparison of the results obtained by two independent theoretical approaches (i.e., the HFR + CPOL + CPEN and the MCDF approximations). The good agreement that was observed indicates that the scale of radiative decay rates is firmly established. This new set of results is expected to help the astrophysicists in the investigation of vacuum ultraviolet high resolution spectra and hopefully will contribute to throwing some light on nucleosynthesis processes regarding the production of heavy elements in metal-poor stars. Note that four of our newly tabulated Te II lines were recently used to deduce the tellurium abundance in Sirius [81].

4.2. Sixth row elements

The sixth row of the periodic table includes the elements Cs (*Z* = 55), Ba (*Z* = 56), and Hf (*Z* = 72) up to Rn (*Z* = 86). Their ground electronic configurations are given in Table 5 for the first three ionization stages. From Hf, with a common [Xe]$4f^{14}$ ionic core, these elements progressively fill their 6s, 5d, and 6p subshells in a rather irregular way along the period due to similar energies of the 6s and 5d orbitals. In some cases, this makes very complicated isoelectronic investigations of the atomic structure because the ground configurations are not even the same for the first three members of the sequences. This is, for instance, the case for Hf-, Ta-, Re-, and Os-like ions for which the ground configurations are of the type $5d^k6s^2$, $5d^{k+1}6s$ and $5d^{k+2}$ (k = 2, 3, 5, 6) for the neutral, the singly ionized, and the doubly ionized atoms, respectively, along the isoelectronic sequences. The results obtained in our work up to now concerning the radiative parameters in the sixth row elements are presented in Table 6. Experimental and theoretical details are given in the different references listed in the table. Hereinafter, we summarize the most recent investigations performed over the past 5 years.

Very interesting experimental data on Hf II lifetimes, transition probabilities, and oscillator strengths were given some years ago

Table 6. Experimental and theoretical methods used in our work for the determination of radiative parameters in sixth row elements (*Z* = 55–56, 72–86) and related references.

Z	Ion	Experimental method[a]	Theoretical method[b]	References
55	Cs VIII	—	HFR, MCDF	[62]
56	Ba I	TR-LIF	HFR	[82]
	Ba II	HISR	HFR	[43]
	Ba IV	—	HFR	[184]
	Ba V	—	HFR	[184]
	Ba VI	—	HFR	[184]
	Ba VII	—	HFR	[184]
	Ba IX	—	HFR, MCDF	[62]
72	Hf I	TR-LIF	HFR	[83]
	Hf II	—	HFR, OPS	[103]
	Hf III	TR-LIF	HFR	[83]
73	Ta I	TR-LIF	HFR	[84]
	Ta II	TR-LIF	HFR	[85]
	Ta III	TR-LIF	HFR	[86]
74	W I	—	HFR	[104]
		—	HFR	[105]
	W II	—	HFR	[104]
		TR-LIF	HFR	[106]
	W III	—	HFR	[104]
		TR-LIF	HFR	[107]
	W IV	—	HFR, MCDF	[108]
	W V	—	HFR, MCDF	[109]
	W VI	—	HFR, MCDF	[110]
	W VIII	—	HFR	[111]
75	Re I	TR-LIF	HFR	[87]
	Re II	TR-LIF	HFR	[88]
76	Os I	—	MCDF	[120]
		TR-LIF	HFR	[89]
	Os II	TR-LIF	HFR	[89]
77	Ir I	TR-LIF	HFR	[90]
	Ir II	TR-LIF	HFR	[90]
78	Pt II	TR-LIF	HFR	[91]
79	Au I	TR-LIF	HFR	[92]
	Au II	TR-LIF	HFR	[92]
		LIBS	HFR	[93]
		LIBS	HFR	[35]
	Au III	—	HFR	[94]
80	Hg I	TR-LIF	HFR	[95]
81	Tl I	TR-LIF	HFR	[96]
82	Pb I	TR-LIF	HFR	[97]
		TR-LIF	HFR	[98]
	Pb II	TR-LIF	MCDF	[99]
83	Bi II	—	HFR, MCDF	[100]
	Bi III	—	MCDF	[99]
84	Po I	—	HFR	[115]

[a]Experimental methods used in our work; TR-LIF, time-resolved laser-induced-fluorescence; LIBS, laser induced-breakdown spectroscopy; BFS, beam–foil spectroscopy; HISR, heavy-ion storage ring.

[b]Theoretical methods used in our work: HFR, pseudo-relativistic Hartree–Fock (including CPOL and CPEN contributions or including core–valence correlation explicitly); OPS, oscillator strength parametrization; MCDF, multiconfiguration Dirac–Fock.

[101, 102] but unfortunately without any theoretical background. In our work we have compared these experimental values with computed ones obtained using two independent semi-empirical methods (i.e., the HFR + CPOL + CPEN approach and the OSP technique in collaboration with Prof. S. Bouazza (Reims, France)) [103]. The overall agreement between all sets of data was found to be good. We furthermore computed radial integrals of the main atomic transitions in this study: $\langle 5d6s6p|r^1|5d^26s\rangle$ = 0.1504 ± 0.0064, $\langle 6s^26p|r^1|5d6s^2\rangle$ = 1.299 ± 0.012, $\langle 5d^26p|r^1|5d^26s\rangle$ = −0.298 ± 0.013, $\langle 5d^26p|r^1|5d^3\rangle$ = 2.025 ± 0.027. Finally our investigation of singly ionized hafnium was extended by comparing our calculated oscillator strengths with available experimental data and by predicting new values for a rather large number of transitions.

Among the sixth row elements considered in our work, tungsten (Z = 74) deserves particular attention. Indeed, it is well known that spectroscopic parameters of W ions are essential for exploring the physical conditions in tokamak plasmas, such as ITER, in which tungsten is currently considered to be a primary candidate for the plasma-facing material in the divertor region. In fusion reactors, tungsten will be sputtered from the wall as a neutral element and the determination of the W influx rate to the core plasma will depend on a calculation of transport from the wall surface through the scrape-off layer. Consequently, the identification of emission lines and the knowledge of radiative parameters from all ionization stages of tungsten will greatly aid modelling of the plasma edge and scrape-off layer transport and facilitate the analysis of net tungsten influx rates. In this context, the new sets of atomic data obtained in our work for the first ionization stages of tungsten (W I, W II, and W III) [104–107] will be extremely useful for future fusion plasma analyses. As an extension of these studies, radiative decay rates have been obtained recently for allowed (E1) and forbidden (M1, E2) transitions in Lu-like (W IV), Yb-like (W V), Tm-like (W VI), and Ho-like (W VIII) tungsten [108–111]. The latter investigations were carried out with the HFR + CPOL + CPEN method in which the radial energy parameters were optimized semi-empirically using the most recent experimental energy levels available (ref. 112 for W IV–VI and ref. 113 for W VIII), allowing us to reproduce the observed level structures with an accuracy of a few hundreds of inverse centimetres at the most. Our calculations have illustrated in a convincing way the importance of core–valence correlation effects, which substantially increase the lifetimes and, accordingly, decrease the transition probabilities of these heavy ions. Because of the lack of experimental data, the reliability of the theoretical A-values could only be tested by comparison of numerical results obtained with independent methods, such as the HFR approach including CPOL and CPEN corrections (HFR + CPOL + CPEN), the MCDF method, and the Flexible Atomic Code (FAC) [114], well suited for investigating the atomic structure of heavy ions. From detailed comparisons between these different approaches, the accuracy of the computed transition probabilities and oscillator strengths has been estimated. While the excellent agreement between the different sets of transition rates gave us confidence in the precision of the results obtained, for a few lines the different methods led to rather large discrepancies, up to a factor of 2. However, it has been shown that such discrepancies arose because of very high sensitivity of the oscillator strengths to the wavefunction mixings, which are expected to be better estimated when using semi-empirical methods. A typical example is given in Table 7 for the $5d^2\ {}^1G_4$–$5d6p\ {}^3F_4$ intercombination line in W V, for which a large discrepancy was observed between the semi-empirical HFR + CPOL + CPEN and ab initio MCDF results [109]. This transition is in fact driven by the $5d^2\ {}^3F_4$ component in $5d^2\ {}^1G_4$ state. Although this admixture is only of a few percent, the small difference between the HFR + CPOL + CPEN wavefunction (91% ^{1}G + 9% ^{3}F) and the MCDF one (94% ^{1}G + 6% ^{3}F) explains the discrepancy by a factor of 1.7 between the gf-values, as shown in the table. Indeed, when modifying the HFR + CPOL + CPEN wavefunctions (by slightly changing the numerical values of Slater integrals) to reproduce the MCDF mixing, an excellent agreement was observed between the oscillator strengths.

Table 7. Influence of the level mixing on the calculated oscillator stregth (gf) of the $5d^2\ {}^1G_4$–$5d6p\ {}^3F_4$ transition in W V. The details of the calculations are given in ref. 109.

Method	Mixing of $5d^2\ {}^1G_4$	gf
HFR+CPOL+CPEN	91% ^{1}G+9% ^{3}F	0.093
	92% ^{1}G+8% ^{3}F	0.081
	93% ^{1}G+7% ^{3}F	0.072
	94% ^{1}G+6% ^{3}F	0.057
MCDF	94% ^{1}G+6% ^{3}F	0.056

It is important to note that the results obtained in our work for tungsten ions represent one of the main sources of spectroscopic properties used in the Atomic Data and Analysis Structure (ADAS) Project (http://www.adas-fusion.eu). The major goal of this project consists of the implementation of atomic data in plasma diagnostics and modeling at fusion laboratories throughout Europe in the context of ITER development.

The electronic structure of highly radioactive polonium (Z = 84) is among the most poorly known of all the neutral atoms of the periodic table. To start to address this lack of data, and as a support to future experimental or theoretical studies, we performed atomic structure calculations on Po I using a theoretical approach including a large amount of electronic correlation and the most important relativistic effects [115]. More precisely, different models based on the HFR method were used for the first time for modelling the atomic structure and for computing radiative parameters involving the lowest states within the $6p^4$, $6p^36d$, $6p^37s$, $6p^37p$, and $6p^37d$ configurations of neutral polonium. This work allowed us to fix the spectroscopic designation of some experimental energy levels not clearly classified in previous analyses and to provide a set of new reliable oscillator strengths corresponding to 31 Po spectral lines in the wavelength region from 175 to 987 nm. The new identifications were facilitated by comparing the available experimental spectral line positions and intensities [116, 117] with computed wavelengths and weighted transition probabilities, as illustrated in Fig. 2. Our study also emphasized the dominating influence of core–valence and core–core correlation for the $6p^4$–$6p^36d$ and $6p^4$–$6p^37s$ transitions. This new investigation is expected to provide a theoretical support to laser-spectroscopy experiments at ISOLDE [118] and to check other theoretical methods that will be used to compute hyperfine structure and isotope shift electronic parameters in the future. In addition, the new set of oscillator strengths obtained in our work provides the basic information for a quantitative analysis of the polonium content in some chemically peculiar stars [119].

The optical data of hyperfine structure and (or) isotope shifts for any element are used mainly to test atomic theory, to deduce nuclear moments and changes in the nuclear mean square charge radius, and to give information on electron behaviour inside the atom. In this context, it is worth mentioning our recent theoretical analysis of isotope shifts in neutral osmium (Z = 76) [120]. In this latter study, the normal mass shift, specific mass shift, and field shift electronic parameters, have been calculated for all the fine-structure levels of the $5d^8$, $5d^76s$, and $5d^66s^2$ even configurations of Os I using the fully relativistic MCDF method. These values can be used to determine the line and level shifts for any pair of neutral osmium isotopes. Comparisons with the experimental fine-structure level shifts by Kröger et al. [121] for the isotope pair ^{190,192}Os I revealed good agreement with our theoretical predictions.

Fig. 2. Comparison of the calculated HFR wavelengths and weighted transition probabilities (g*A*) [115] with the experimental spectrum taken from the NIST compilation for the polonium atom (Po I) [117].

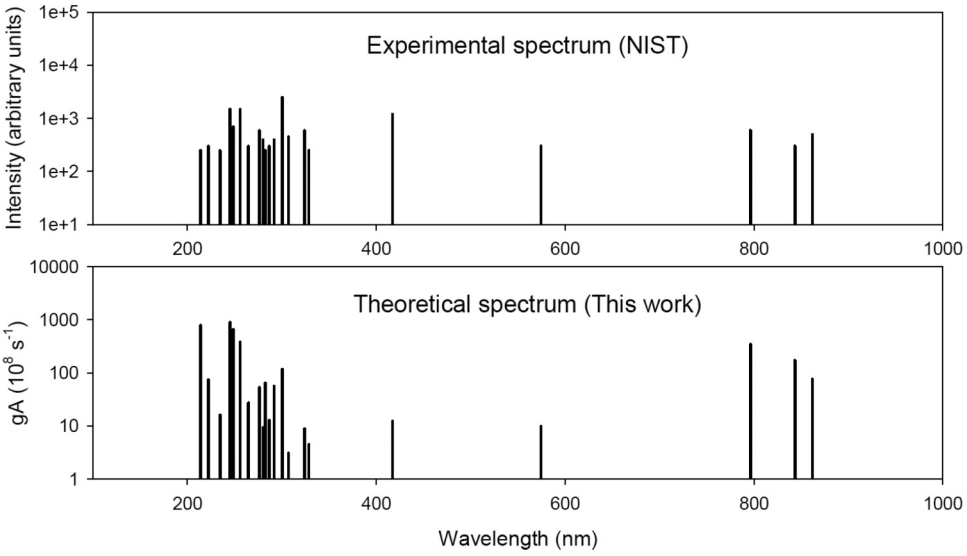

4.3. Lanthanide elements

Many efforts to improve our knowledge of the atomic structure and radiative properties of the lanthanides (i.e., the elements ranging from La (Z = 57) to Lu (Z = 71)) carried out during the past 20 years have already been described and thoroughly discussed in different review papers [17–19] in which the experimental and theoretical difficulties related to the study of these elements were highlighted. To summarize, let us recall that the neutral and slightly ionized lanthanides are characterized by the progressive filling of the 4f subshell, having a common feature of a xenon structure with, in addition, two or three 5d and (or) 6s electrons. The ground configurations for the first three ionization stages are listed in Table 8. The energy and spatial extension of the 4f eigenfunction drop suddenly at the beginning of the lanthanide sequence in such a way that, if the 4f wavefunction is still essentially located outside the xenon core in lanthanum (Z = 57), its maximum lies deeply inside the $5s^25p^6$ closed subshells in neodymium (Z = 60). In view of the imperfect screening of the 4f electrons, this collapse is very rapid with increasing atomic number (i.e., with the increasing number of 4f electrons). Moreover, these elements are characterized by low-lying configurations of the types $4f^k$, $4f^{k-1}nl$, $4f^{k-2}nln'l'$ and $4f^{k-3}nln'l'n''l''$. These configurations not only give rise to a huge number of energy levels but they also often overlap each other leading to strong interactions. This is illustrated in Fig. 3 showing the overlap of the lowest odd-parity configurations in Er II (Z = 68). On the experimental side, the lanthanide atoms and ions greatly suffer from the poor knowledge of classified spectral lines and established energy levels, as already emphasized in many of our papers (see, e.g., ref. 17–19). This imposes a severe limitation on the use of semi-empirical methods for modelling the corresponding atomic structures and computing the radiative parameters. New term analyses in the laboratory would therefore be very welcome. We notice however with satisfaction that some effort has recently been made in that direction, as, for example, by Wyart and coworkers who used the Racah–Slater parametric method for classifying a number of energy levels in strongly mixed configurations of complex ions, such as Nd II [122, 123], Er II [124], and Tm II [123]. These new results should motivate more elaborate theoretical or semi-empirical works in the future.

The results we have obtained so far concerning the determination of radiative data in lanthanide elements are listed in Table 9.

Table 8. Ground configurations for the first three ionization stages of lanthanide atoms.

		Ground configuration		
Z	Element	I	II	III
57	La	$5d6s^2$	$5d^2$	5d
58	Ce	$4f5d6s^2$	$4f5d^2$	$4f^2$
59	Pr	$4f^36s^2$	$4f^36s$	$4f^3$
60	Nd	$4f^46s^2$	$4f^46s$	$4f^4$
61	Pm	$4f^56s^2$	$4f^56s$	$4f^5$
62	Sm	$4f^66s^2$	$4f^66s$	$4f^6$
63	Eu	$4f^76s^2$	$4f^76s$	$4f^7$
64	Gd	$4f^75d6s^2$	$4f^75d6s$	$4f^75d$
65	Tb	$4f^96s^2$	$4f^96s$	$4f^9$
66	Dy	$4f^{10}6s^2$	$4f^{10}6s$	$4f^{10}$
67	Ho	$4f^{11}6s^2$	$4f^{11}6s$	$4f^{11}$
68	Er	$4f^{12}6s^2$	$4f^{12}6s$	$4f^{12}$
69	Tm	$4f^{13}6s^2$	$4f^{13}6s$	$4f^{13}$
70	Yb	$4f^{14}6s^2$	$4f^{14}6s$	$4f^{14}$
71	Lu	$4f^{14}5d6s^2$	$4f^{14}6s^2$	$4f^{14}6s$

Until very recently, we had mainly concentrated on the determination of atomic data of neutral, singly or doubly ionized lanthanides in view of their astrophysical interest. Because of their unusual luminescent properties, triply charged lanthanide ions find many applications in different fields, such as the lighting industry, photonics, laser physics, and biotechnology [13–16]. If we except La IV, all these ions are characterized by a ground electronic configuration of the type $[Xe]4f^k$ with k varying from 1 (Ce IV) to 14 (Lu IV), which is largely responsible for their interesting photophysical properties, such as long-lived luminescence and sharp absorption and emission lines. Understanding the light emission from triply charged lanthanides requires reliable information about their atomic structures and radiative parameters. However, our knowledge of the spectra corresponding to these ions is still very fragmentary. Indeed, up to a recent past, their radiative properties were essentially investigated from spectroscopy experiments on ions embedded in compounds or crystal lattices. Following our previous investigations of La IV [39], Ce IV [159], and Yb IV [160], we have recently extended the theoretical analysis of trebly ionized lanthanide atoms by considering the

Fig. 3. Low-lying odd-parity configurations in Er II, as computed by the HFR method.

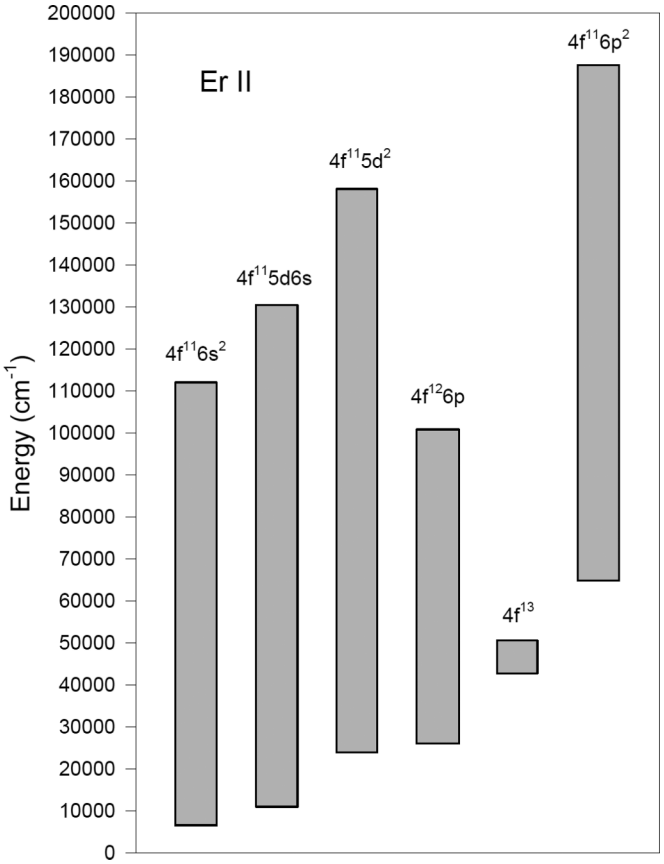

Pr IV [161] and Nd IV [162] ions. For Pr IV, transition probabilities and oscillator strengths for electric dipole radiation were reported for the first time. They were computed using a semi-empirical HFR approach including CPOL effects, by assuming the atomic system as two valence electrons surrounding a xenon-like Pr VI closed shell ionic core. Because of the lack of experimental data in this ion, the accuracy of our results was estimated and discussed on the basis of comparisons between calculations performed with a similar physical model and laboratory measurements previously published for the isoelectronic ion Ce III [163]. In view of their great interest in optical materials and nanophotonics, radiative rates for forbidden lines within the 4f^2 ground-state configuration of Pr IV were also calculated in our work. The case of Nd IV appeared a bit more complicated because some core–excited configurations with an open 5p subshell were expected to strongly interact with lower configurations. In particular, we showed the dramatic increasing influence of the 5p^{5}4f^4 configuration along the lanthanum isoelectronic sequence meaning that, if the CPOL potential could be used to model core–valence interactions in previous La-like Ce II and Pr III ions, this approach was no more valid in Nd IV for which core–excited configurations with an open 5p subshell had to be included explicitly in the multiconfiguration expansions. Using a rather extended physical model, a new set of radiative parameters has been obtained for electric dipole, magnetic dipole, and electric quadrupole lines and compared with other available theoretical data. For electric dipole transitions, our results are expected to be more accurate than those previously published in view of the much more extended amount of electronic correlation effects (including core–excited correlation) considered in our physical model. In the case of magnetic dipole and electric quadrupole lines, our results have been found to be in good agreement with theoretical data recently published for the most intense transitions [164].

Table 9. Experimental and theoretical methods used in our work for the determination of radiative parameters in lanthanide elements (Z = 57–71) and related references.

Z	Ion	Experimental method[a]	Theoretical method[b]	References
57	La I	TR-LIF	HFR	[125]
	La III	TR-LIF	HFR	[126]
	La IV	BFS	HFR, MCDF	[39]
58	Ce II	—	HFR	[127]
		TR-LIF	HFR	[128]
	Ce III	—	HFR	[163]
	Ce IV	TR-LIF	HFR	[159]
59	Pr I	TR-LIF	HFR	[129]
	Pr II	TR-LIF	HFR	[130]
	Pr III	—	HFR	[131]
		TR-LIF	HFR	[132]
	Pr IV	—	HFR	[161]
60	Nd I	TR-LIF	HFR	[129]
	Nd II	TR-LIF	HFR	[133]
		HISR	HFR, MCDF	[134]
	Nd III	TR-LIF	HFR	[135]
	Nd IV	—	HFR	[162]
61	Pm II	—	HFR	[136]
		—	HFR	[137]
62	Sm II	TR-LIF	HFR	[138]
	Sm III	TR-LIF	HFR	[139]
63	Eu III	TR-LIF	HFR	[140]
64	Gd III	—	HFR	[141]
65	Tb III	TR-LIF	HFR	[142]
66	Dy III	TR-LIF	HFR	[143]
67	Ho III	TR-LIF	HFR	[144]
		TR-LIF	HFR	[145]
68	Er II	TR-LIF	HFR	[146]
	Er III	TR-LIF	HFR	[147]
69	Tm II	—	HFR	[148]
	Tm III	TR-LIF	HFR	[149]
70	Yb II	—	HFR	[150]
		—	HFR	[151]
		TR-LIF	HFR	[152]
		TR-LIF	HFR	[153]
	Yb III	TR-LIF	HFR	[154]
		TR-LIF	HFR	[155]
	Yb IV	—	HFR	[160]
71	Lu I	TR-LIF	HFR	[156]
		TR-LIF	HFR	[157]
	Lu II	TR-LIF	HFR	[156]
		TR-LIF	HFR	[158]
	Lu III	TR-LIF	HFR	[126]
		TR-LIF	HFR	[156]

[a]Experimental methods used in our work: TR-LIF, time-resolved laser-induced-fluorescence; BFS, beam–foil spectroscopy; HISR, heavy-ion storage ring.

[b]Theoretical methods used in our work: HFR, pseudo-relativistic Hartree–Fock (including CPOL and CPEN contributions or including core–valence correlation explicitly); MCDF, multiconfiguration Dirac–Fock.

4.4. Seventh row elements and actinides

As an extension of our early work on the francium atom (Z = 87) [165] towards ionized elements along the isoelectronic sequence, radiative rates have been computed in Ra II (Z = 88), Ac III (Z = 89), Th IV (Z = 90), and U VI (Z = 92) ions. Motivations for investigating Th IV in particular relied on the fact that ^{229}Th nucleus has an optical transition at 3.5 eV that may make an excellent optical clock and that this ion has also very interesting properties for

nuclear laser spectroscopy [166]. Francium-like ions have a rather simple atomic structure with one outer electron moving in the resultant field of the nucleus and the 86 inner electrons. This represented therefore a very good opportunity to check both the relativistic and core–valence correlation effects by comparing the results obtained with the HFR + CPOL + CPEN and MCDF approaches [167].

In astrophysics, observations have suggested the presence of short-lived radioactive elements, such as $84 \leq Z \leq 99$ elements (in addition to Tc (Z = 43) and Pm (Z = 61)) at the surface of the chemically peculiar roAp star HD 101065, also known as Przybylski's star [4, 119, 168, 169]. In particular, Gopka et al. [119] presented the results on new identifications of the lines of all radioactive elements with atomic numbers from Z = 84 to 99, except for Z = 85 (At) and Z = 87 (Fr). The presence of these heavy short-lived radioactive elements in HD 101065 star is enigmatic (see discussion in refs. 4, 119, 168–172). Goriely [173] stressed the importance of spallation nucleosynthesis compared to diffusion processes as a possible explanation of the chemical composition of the outer layers of some chemically peculiar stars. The available astrophysical spectroscopic observations were, however, affected by large uncertainties essentially due to the lack of atomic data for the elements of interest. Among the difficulties to be solved in the actinides, it is worth mentioning that the 5f orbital is less embedded in the core than the 4f orbital in the lanthanides, the predominance of the relativistic effects in the calculation of $nf - (n+1)d$ excitations, the fact that the spectra show few intense lines, and the presence of hyperfine structure effects and isotope shifts. As a first contribution to fill in this gap, oscillator strengths have been calculated for strong lines in neutral and singly ionized radium, Ra I and Ra II (Z = 88) and actinium, Ac I and Ac II (Z = 89). A close examination of the spectra of two peculiar stars (i.e., HD 101065 and HR 465) indicated that some absorption features could possibly be due to Ra II and Ac II [174].

We also calculated transition probabilities for six spectral lines of neutral americium (Z = 99) of potential astrophysical interest [175]. The complexity of the atomic structure of this element, characterized by low-lying and interacting configurations as complex as $5f^6 6d 7s^2$, $5f^7 7s 7p$, $5f^6 6d^2 7s$ (even parity) and $5f^7 7s^2$, $5f^7 6d 7s$, $5f^6 7s^2 7p$, $5f^6 6d 7s 7p$, $5f^7 7s 8s$, $5f^7 6d^2$ (odd parity), imposed severe constraints on the HFR physical model used for the calculation of radiative parameters. The theoretical lifetimes were nevertheless in reasonable agreement with the few experimental data available [176]. This work provided for the first time the basic information for a quantitative investigation of the americium content in some chemically peculiar stars.

Under certain circumstances, the age of a star can be determined by the use of a radioactive isotope of sufficiently long lifetime, and two such isotopes are frequently considered in cosmochronology (i.e., ^{232}Th and ^{238}U, which have half-lives of 14.05 Gyr and 4.47 Gyr, repectively). Because of the complete lack of atomic data, neither Th III nor UIII lines had been considered in the analysis of astrophysical spectra until the first determination of radiative parameters we published a few years ago [177, 178]. In these works, experimental lifetime measurements for six levels in Th III and five levels in U III were combined with theoretical branching fractions to obtain new transition probabilities. As an example of direct astrophysical application of these results, two lines identified as Th III could be observed and used to estimate the thorium abundance in the atmosphere of the rapidly oscillating Ap star HD 24712 [179].

All the results obtained in our work concerning the radiative data in seventh-row and actinide elements are compiled in Table 10.

Table 10. Experimental and theoretical methods used in our work for the determination of radiative parameters in seventh row elements and actinides, and related references.

Z	Ion	Experimental method[a]	Theoretical method[b]	References
87	Fr I	—	HFR	[165]
88	Ra I	—	HFR	[174]
	Ra II	—	HFR, MCDF	[167]
		—	HFR	[174]
89	Ac I	—	HFR	[174]
	Ac II	—	HFR	[174]
	Ac III	—	HFR, MCDF	[167]
90	Th III	TR-LIF	HFR	[177]
	Th IV	—	HFR, MCDF	[167]
91	Pa V	—	HFR, MCDF	[167]
92	U III	TR-LIF	HFR	[178]
	U VI	—	HFR, MCDF	[167]
95	Am I	—	HFR	[175]

[a]Experimental methods used in our work: TR-LIF, time-resolved laser-induced-fluorescence.

[b]Theoretical methods used in our work: HFR, pseudo-relativistic Hartree–Fock (including CPOL and CPEN contributions or including core–valence correlation explicitly); MCDF, multiconfiguration Dirac–Fock.

5. New oscillator strengths for three- to six-times ionized heavy atoms and their application in white dwarf analysis

An interesting astrophysical application of the new radiative parameters recently obtained in our work for some moderately ionized heavy atoms is illustrated in this section. More precisely, in 2012, Werner et al. [180] identified many spectral lines of trans-iron heavy metals, such as Zn (Z = 30), Ga (Z = 31), Ge (Z = 32), As (Z = 33), Se (Z = 34), Kr (Z = 36), Mo (Z = 42), Sn (Z = 50), Te (Z = 52), I (Z = 53), Xe (Z = 54), and Ba (Z = 56) in the high-resolution ultraviolet spectrum of the hot DO-type white dwarf RE 0503–289 (effective temperature $T_{\rm eff}$ = 70 000 ± 2000 K, surface gravity log$g$ = 7.5 ± 0.1 cms^{-2}). Based on atomic data available at that time, these authors could determine large overabundances (up to four orders of magnitude larger than the solar values) for Kr and Xe only. The most serious problem for the determination of abundances for the other elements was the lack of radiative data. It is worth noting that non-local thermodynamic equilibrium stellar atmosphere modeling is necessary for such astrophysical objects and therefore oscillator strengths are required not only for the observed line transitions but also for the entire set of lines that need to be considered in the model atoms. To fill this lack of atomic data, we recently started to compute transition rates for spectral lines belonging to three- through six-times ionized elements of interest using the HFR + CPOL + CPEN method. These studies allowed us to provide a large number of new reliable gf-values in Zr IV–VII [181], Mo IV–VII [182], Xe IV–VII [181, 183], and Ba IV–VII [184] fifth- and sixth-row ions, in addition to Zn IV–VII [185], Ga IV–VII [186], Ge IV–VII [187], and Kr IV–VII [188] lighter ions. All these analyses, performed in collaboration with the Institute for Astronomy and Astrophysics of Eberhard Karls University in Tübingen, Germany, showed that, without exception, the abundances of those heavy metals in RE 0503–289 are unexpectedly strong supersolar (up to about 5 dex). This is much higher than predicted by asymptotic giant branch nucleosynthesis calculations indicating that the interplay of gravitational settling and radiative levitation may play an important role for their photospheric prominence.

6. Related online databases

6.1. DREAM

The main purpose of DREAM (database on rare-earths at Mons University), initially introduced in refs. 189, 190, is to provide the

scientific community with information concerning the radiative parameters for the lowest ionization stages of lanthanide atoms. This database is accessible at the address http://hosting.umons.ac.be/html/agif/databases/dream.html. In the tables, the spectra are classified in order of increasing Z values and, for a given Z, according to the ionization degree. For each spectrum, the tables show, the wavelengths (in Å) derived from the available experimental energy levels, the lower and upper levels of the transitions (in cm^{-1}), the weighted oscillator strengths (log*gf*) and transition probabilities (*gA*) calculated using the HFR + CPOL + CPEN method, and the cancellation factors as defined by Cowan [21]. To date, data are tabulated for La III, Ce II, Ce III, Pr II, Pr III, Pr IV, Nd II, Nd III, Sm II, Eu III, Gd III, Tb III, Dy III, Ho III, Er II, Er III, Tm II, Tm III, Yb II, Yb III, Yb IV, Lu I, Lu II, and Lu III.

6.2. DESIRE

DESIRE (database on sixth-row elements) contains information concerning the wavelengths, the oscillator strengths, and the transition probabilities for spectral lines of neutral and slightly ionized sixth-row elements. The format of the tables as well as the methods used for obtaining the listed values are the same as for DREAM. The database, originally presented in ref. 191, is hosted at http://hosting.umons.ac.be/html/agif/databases/desire.html. Until now, radiative data are tabulated for Hf II, Ta I, W I, W II, W III, Os I, Os II, Ir I, and Ir II. In addition, the database contains information about the Landé *g*-factors for the ions Ta I, Ta II, Ta III, W II, W III, Re I, Re II, Os I, Os II, Ir I, Ir II, Pt II, Au I, Au II, Pb I, and Pb II. Note that both DREAM and DESIRE databases are part of the Virtual Atomic and Molecular Data Centre (VAMDC) Consortium [192].

6.3. TOSS

The database TOSS (Tübingen oscillator strengths service) provides oscillator strengths and transition probabilities for moderately ionized heavy atoms. Mainly based on experimental energy levels, these were calculated with the semi-empirical HFR + CPOL + CPEN approach in accordance with the procedures described in detail in our different papers related to the search (and identification) of trans-iron elements in the hot white dwarfs G191-B2B and RE0503–289 [181–188]. More precisely, new radiative parameters for tens of thousands spectral lines in moderately charged fifth- and sixth-row ions, such as Zr IV–VII, Mo IV–VII, Tc IV–VII, Xe IV–VII, and Ba IV–VII, in addition to new atomic data obtained for the lighter ions Zn IV–VII, Ga IV–VII, Ge IV–VII, and Kr IV–VII are currently available in the database. The TOSS service is part of the German Astrophysical Virtual Observatory and is accessible at the address http://dc.g-vo.org/TOSS.

7. Conclusion

Thanks to our systematic and detailed investigations, the knowledge of the atomic structures and radiative properties of heavy atoms and ions, typically ranging from $Z = 37$ to 95, has considerably progressed during the past 20 years, giving rise to about 150 papers that are collected in the present review. This big effort was made possible by the use of independent semi-empirical and theoretical methods the reliability of the results of which was in most cases assessed through comparisons with accurate experimental measurements. The new spectroscopic parameters obtained in our work for hundreds of thousands of lines belonging to more than 120 different atomic systems provide the scientific community with a substantial amount of information needed for the development of research in many various fields, such as astrophysics, plasma physics, laser physics, material science, lighting industry, photonics, biotechnology, and so on.

Acknowledgements

The author would like to thank several collaborators who have been involved in different parts of the works presented in this review. The theoretical calculations were mainly carried out in collaboration with E. Biémont, J. Deprince, V. Fivet, and P. Palmeri at Mons University in Belgium. Special thanks are additionally due to S. Enzonga Yoca from Marien Ngouabi University of Brazzavile, Congo, and S. Bouazza from University of Reims-Champagne-Ardenne, France, for their contributions. The experimental part of many studies reported in the present paper benefited from collaborations with L. Engström, H. Hartman, H. Lundberg, H. Nilsson, and S. Svanberg from Lund University, Sweden; S. Mannervik from Stockholm University, Sweden; K. Blagoev and G. Malcheva from the Bulgarian Academy of Sciences of Sofia, Bulgaria; Z.W. Dai from Jilin University at Changchun, China; R. Mayo and M. Ortiz from Complutense University of Madrid, Spain; and H.P. Garnir from Liège University, Belgium. Acknowledgements are also owed to collaborators from Brussels University in Belgium (A. Jorissen, S. Van Eck) and from Eberhard Karls University of Tübingen in Germany (T. Rauch and their group) for specific applications of our atomic data in astrophysics. The Author is Research Director of the Belgian Fund for Scientific Research F.R.S.-FNRS from which financial support is gratefully acknowledged, as well as from LASERLAB-EU and ADAS-EU Consortiums.

References

1. S. Goriely and B. Clerbaux. Astron. Astrophys. **346**, 798 (1999).
2. A. Jorissen. Phys. Scr. T, **112**, 73 (2004). doi:10.1238/Physica.Topical.112a00073.
3. S.J. Adelman, C.R. Proffitt, G.M. Wahlgren, D.S. Leckrone, and L. Dolk. Astrophys. J. Suppl. Ser. **155**, 179 (2004). doi:10.1086/424802.
4. C.R. Cowley, W.P. Bidelman, S. Hubrig, G. Mathys, and D.J. Bord. Astron. Astrophys. **419**, 1087 (2004). doi:10.1051/0004-6361:20035726.
5. C.R. Cowley, S. Hubrig, P. Palmeri, P. Quinet, E. Biémont, G.M. Wahlgren, O. Schütz, and J.F. Gonzalez. Mon. Not. Roy. Astron. Soc. **405**, 127 (2010).
6. G. Federici, C.H. Skinner, J.N. Brooks, et al. Nucl. Fusion, **41**, 1967 (2001). doi:10.1088/0029-5515/41/12/218.
7. R. Neu, R. Dux, A. Kallenbach, et al. Nucl. Fusion, **45**, 209 (2005). doi:10.1088/0029-5515/45/3/007.
8. A. Pospieszczyk. Nuclear fusion research. Springer, Berlin. 2006.
9. C.H. Skinner. Can. J. Phys. **86**, 285 (2008). doi:10.1139/P07-100.
10. C.H. Skinner. Phys. Scr. T, **134**, 014022 (2009). doi:10.1088/0031-8949/2009/T134/014022.
11. B. Lipschultz, Y. Lin, M.L. Reinke, et al. Phys. Plasmas, **13**, 056117 (2006). doi:10.1063/1.2180767.
12. Z.X. Liu, X. Gao, S.C. Liu, et al. Nucl. Fusion, **53**, 073041 (2013). doi:10.1088/0029-5515/53/7/073041.
13. I. Hemmilä. J. Alloys Comp. **225**, 480 (1995). doi:10.1016/0925-8388(94)07069-5.
14. B.G. Wybourne. J. Alloys Comp. **380**, 96 (2004). doi:10.1016/j.jallcom.2004.03.034.
15. Y. Hasegawa, Y. Wada, and S. Yanagida. J. Photochem. Photobiol. C: Photochem. Rev. **5**, 183 (2004). doi:10.1016/j.jphotochemrev.2004.10.003.
16. A. Døssing. Eur. J. Inorg. Chem. **2005**, 1425 (2005). doi:10.1002/ejic.200401043.
17. P. Quinet, P. Palmeri, E. Biémont, Z.S. Li, S. Zhang, and Svanberg. J. Alloys Comp. **344**, 255 (2002). doi:10.1016/S0925-8388(02)00363-8.
18. E. Biémont and P. Quinet. Phys. Scr. T, **105**, 38 (2003).
19. E. Biémont. Phys. Scr. T, **119**, 55 (2005). doi:10.1088/0031-8949/2005/T119/010.
20. E. Biémont. *In* New trends in atomic and molecular physics. Springer Series on Atomic, Optical and Plasma Physics **76**, 1 (2013). doi:10.1007/978-3-642-38167-6_1.
21. R.D. Cowan. The theory of atomic structure and spectra. University of California Press, Berkeley. 1981.
22. J. Migdalek and W.E. Baylis. J. Phys. B: Atom. Mol. Phys. **11**, L497 (1978). doi:10.1088/0022-3700/11/17/001.
23. S. Fraga, J. Karwowski, and K.M.S. Saxena. Handbook of atomic data. Elsevier, Amsterdam. 1976.
24. W.R. Johnson, D. Kolb, and K.-N. Huang. Atom. Data Nucl. Data Tables, **28**, 333 (1983). doi:10.1016/0092-640X(83)90020-7.
25. S. Hameed, A. Herzenberg, and M.G. James. J. Phys. B: Atom. Mol. Phys. **1**, 822 (1968). doi:10.1088/0022-3700/1/5/308.
26. S. Hameed. J. Phys. B, **5**, 746 (1972). doi:10.1088/0022-3700/5/4/009.
27. J. Ruczkowski, M. Elantkowska, and J. Dembczyński. J. Quant. Spectrosc. Radiat. Transf. **145**, 20 (2014). doi:10.1016/j.jqsrt.2014.04.018.
28. I.P. Grant, B.J. McKenzie, P.H. Norrington, D.F. Mayers, and N.C. Pyper. Comput. Phys. Commun. **21**, 207 (1980). doi:10.1016/0010-4655(80)90041-7.
29. B.J. McKenzie, I.P. Grant, and P.H. Norrington. Comput. Phys. Commun. **21**, 233 (1980). doi:10.1016/0010-4655(80)90042-9.
30. I.P. Grant. Relativistic quantum theory of atoms and molecules. Springer. 2007.

31. K.G. Dyall, I.P. Grant, C.T. Johnson, F.A. Parpia, and E.P. Plummer. Comput. Phys. Commun. **55**, 425 (1989). doi:10.1016/0010-4655(89)90136-7.
32. P. Jönsson, X. He, C. Froese Fischer, and I.P. Grant. Comput. Phys. Commun. **177**, 597 (2007). doi:10.1016/j.cpc.2007.06.002.
33. P. Jönsson, J. Gaigalas, J. Bieroń, C. Froese Fischer, and I.P. Grant. Comput. Phys. Commun. **184**, 2197 (2013). doi:10.1016/j.cpc.2013.02.016.
34. L. Engström, H. Lundberg, H. Nilsson, H. Hartman, and E. Bäckström. Astron. Astrophys. **570**, A34 (2014). doi:10.1051/0004-6361/201424762.
35. É. Biémont, K. Blagoev, V. Fivet, G. Malcheva, R. Mayo, M. Ortiz, and P. Quinet. Mon. Not. Roy. Astron. Soc. **380**, 1581 (2007). doi:10.1111/j.1365-2966.2007.12200.x.
36. É. Biémont, V. Buchard, H.-P. Garnir, P.-H. Lefebvre, and P. Quinet. Eur. Phys. J. D, **33**, 181 (2005). doi:10.1140/epjd/e2005-00059-y.
37. É. Biémont, M. Clar, V. Fivet, H.-P. Garnir, P. Palmeri, P. Quinet, and D. Rostohar. Eur. Phys. J. D, **44**, 23 (2007). doi:10.1140/epjd/e2007-00161-2.
38. H.-P. Garmir, S. Enzonga Yoca, P. Quinet, and E. Biémont. J. Quant. Spectrosc. Rad. Transfer. **110**, 284 (2009). doi:10.1016/j.jqsrt.2008.11.007.
39. É. Biémont, M. Clar, S. Enzonga Yoca, V. Fivet, P. Quinet, E. Träbert, and H.-P. Garnir. Can. J. Phys. **87**, 1275 (2009). doi:10.1139/P09-105.
40. S. Mannervik. Phys. Scr. T, **100**, 81 (2002).
41. S. Mannervik. Phys. Scr. T, **105**, 67 (2003). doi:10.1238/Physica.Topical.105a00067.
42. P. Schef, P. Lundin, E. Biémont, A. Källberg, L.-O. Norlin, P. Palmeri, P. Royen, A. Simonsson, and S. Mannervik. Phys. Rev. A, **72**, 020501 (2005). doi:10.1103/PhysRevA.72.020501.
43. J. Gurell, E. Biémont, K. Blagoev, V. Fivet, P. Lundin, S. Mannervik, L.-O. Norlin, P. Quinet, D. Rostohar, P. Royen, and P. Schef. Phys. Rev. A, **75**, 052506 (2007). doi:10.1103/PhysRevA.75.052506.
44. É. Biémont, K. Blagoev, L. Engström, H. Hartman, H. Lundberg, G. Malcheva, H. Nilsson, P. Palmeri, and P. Quinet. Mon. Not. R. Astron. Soc. **414**, 3350 (2011). doi:10.1111/j.1365-2966.2011.18637.x.
45. G. Malcheva, R. Mayo, M. Ortiz, J. Ruiz, L. Engström, H. Lundberg, H. Nilsson, P. Quinet, E. Biémont, and K. Blagoev. *In* 15th International School on Quantum Electronics: Laser Physics and Applications. *Edited by* T. Dreischuh, E. Taskova, E. Borisova, and A. Serafetinides. Proc. SPIE, **7027**, 7027M (2008).
46. G. Malcheva, R. Mayo, M. Ortiz, J. Ruiz, L. Engström, H. Lundberg, H. Nilsson, P. Quinet, É. Biémont, and K. Blagoev. Mon. Not. R. Astron. Soc. **395**, 1523 (2009). doi:10.1111/j.1365-2966.2009.14629.x.
47. G. Malcheva, K. Blagoev, R. Mayo, M. Ortiz, H.L. Xu, S. Svanberg, P. Quinet, and E. Biémont. Mon. Not. R. Astron. Soc. **367**, 754 (2006). doi:10.1111/j.1365-2966.2005.09987.x.
48. P. Quinet, S. Bouazza, and P. Palmeri. J. Quant. Spectrosc. Radiat. Transfer, **164**, 193 (2015). doi:10.1016/j.jqsrt.2015.06.011.
49. G. Malcheva, H. Nilsson, L. Engström, H. Lundberg, É. Biémont, P. Palmeri, P. Quinet, and K. Blagoev. Mon. Not. R. Astron. Soc. **412**, 1823 (2011). doi:10.1111/j.1365-2966.2010.18020.x.
50. P. Quinet. J. Phys. B: Atom. Mol. Opt. Phys. **35**, 19 (2002). doi:10.1088/0953-4075/35/1/302.
51. H. Lundberg, L. Engström, H. Hartman, H. Nilsson, P. Palmeri, P. Quinet, and É. Biémont. J. Phys. B: Atom. Mol. Opt. Phys. **43**, 085004 (2010). doi:10.1088/0953-4075/43/8/085004.
52. L. Jiang, Q. Wang, Y. Feng, P. Quinet, É. Biémont, S. Li, and Z. Dai. Eur. Phys. J. D, **66**, 176 (2012). doi:10.1140/epjd/e2012-30228-8.
53. P. Palmeri, P. Quinet, E. Biémont, A.V. Yushchenko, A. Jorissen, and S. Van Eck. Mon. Not. R. Astron. Soc. **374**, 63 (2007). doi:10.1111/j.1365-2966.2006.11016.x.
54. V. Fivet, P. Quinet, P. Palmeri, et al. Mon. Not. R. Astron. Soc. **396**, 2124 (2009). doi:10.1111/j.1365-2966.2009.14761.x.
55. G. Malcheva, L. Engström, H. Lundberg, H. Nilsson, H. Hartman, K. Blagoev, P. Palmeri, and P. Quinet. Mon. Not. R. Astron. Soc. **450**, 223 (2015). doi:10.1093/mnras/stv375.
56. P. Quinet, É. Biémont, P. Palmeri, L. Engström, H. Hartman, H. Lundberg, and H. Nilsson. J. Elec. Spectrosc. Rel. Phen. **184**, 174 (2011). doi:10.1016/j.elspec.2010.08.001.
57. H.L. Xu, Z.W. Sun, Z.W. Dai, Z.K. Jiang, P. Palmeri, P. Quinet, and É. Biémont. Astron. Astrophys. **452**, 357 (2006). doi:10.1051/0004-6361:20054610.
58. P. Quinet. Phys. Scr. **54**, 483 (1996). doi:10.1088/0031-8949/54/5/008.
59. E. Biémont, K. Blagoev, J. Campos, R. Mayo, G. Malcheva, M. Ortiz, and P. Quinet. J. Electr. Spectrosc. Rel. Phen. **144–147**, 27 (2005).
60. E. Biémont, K. Blagoev, J. Campos, R. Mayo, G. Malcheva, M. Ortiz, and P. Quinet. *In* 13th International School on Quantum Electronics: Laser Physics and Applications. *Edited by* P.A. Atanasov, S.V. Gateva, L.A. Avramov, A.A. Serafetinides. Proc. of SPIE, **5830**, 221 (2005).
61. J. Campos, M. Ortiz, R. Mayo, E. Biémont, P. Quinet, K. Blagoev, and G. Malcheva. Mon. Not. R. Astron. Soc. **363**, 905 (2005). doi:10.1111/j.1365-2966.2005.09493.x.
62. E. Biémont, C.F. Ficher, M. Godefroid, P. Palmeri, and P. Quinet. Phys. Rev. A, **62**, 032512 (2000). doi:10.1103/PhysRevA.62.032512.
63. H.L. Xu, A. Persson, S. Svanberg, K. Blagoev, G. Malcheva, V. Pentchev, E. Biémont, J. Campos, M. Ortiz, and R. Mayo. Phys. Rev. A, **70**, 042508 (2004). doi:10.1103/PhysRevA.70.042508.
64. Y. Zhang, J. Xu, W. Zhang, et al. Phys. Rev. A, **78**, 022505 (2008). doi:10.1103/PhysRevA.78.022505.
65. W. Zhang, S. You, C. Sun, et al. Eur. Phys. J. D, **55**, 1 (2009). doi:10.1140/epjd/e2009-00181-x.
66. W. Zhang, Y. Feng, J. Xu, P. Palmeri, P. Quinet, É. Biémont, and Z. Dai. J. Phys. B: Atom. Mol. Opt. Phys. **43**, 205005 (2010). doi:10.1088/0953-4075/43/20/205005.
67. H. Hartman, H. Nilsson, L. Engström, H, P. Lundberg, P. Palmeri, É. Quinet, and Biémont. Phys. Rev. A, **82**, 052512 (2010). doi:10.1103/PhysRevA.82.052512.
68. E. Biémont, P. Quinet, and C.J. Zeippen. Phys. Scr. **71**, 163 (2005). doi:10.1238/Physica.Regular.071a00163.
69. W. Zhang, P. Palmeri, and P. Quinet. Eur. Phys. J. D, **68**, 104 (2014). doi:10.1140/epjd/e2014-50071-1.
70. P. Quinet. Phys. Scr. **90**, 015404 (2015). doi:10.1088/0031-8949/90/1/015404.
71. W. Zhang, P. Palmeri, and P. Quinet. Phys. Scr. **88**, 065302 (2013). doi:10.1088/0031-8949/88/06/065302.
72. W. Zhang, P. Palmeri, P. Quinet, and É. Biémont. Astron. Astrophys. **551**, A136 (2013). doi:10.1051/0004-6361/201220918.
73. H. Nilsson, H. Hartman, L. Engström, H. Lundberg, C. Sneden, V. Fivet, P. Palmeri, P. Quinet, and É. Biémont. Astron. Astrophys. **511**, A16 (2010). doi:10.1051/0004-6361/200913574.
74. P. Palmeri, P. Quinet, V. Fivet, É. Biémont, C.H. Cowley, L. Engström, H. Lundberg, H. Hartman, and H. Nilsson. J. Phys. B: Atom. Mol. Opt. Phys. **42**, 165005 (2009). doi:10.1088/0953-4075/42/16/165005.
75. P. Quinet, E. Biémont, P. Palmeri, L. Engström, H. Hartman, H. Lundberg, and H. Nilsson. Astron. Astrophys. **537**, A74 (2012). doi:10.1051/0004-6361/201118205.
76. C.R. Cowley, M.R. Hartoog, M.F. Aller, and A.P. Cowley. Astrophys. J. **183**, 127 (1973). doi:10.1086/152214.
77. I.U. Roederer, J.E. Lawler, J.J. Cowan, et al. Astrophys. J. **747**, L8 (2012). doi:10.1088/2041-8205/747/1/L8.
78. E. Biémont, J.E. Hansen, P. Quinet, and C.J. Zeippen. Astron. Astrophys. Suppl. **111**, 333 (1995).
79. K. Werel and L. Augustyniak. Phys. Scr. **23**, 856 (1981). doi:10.1088/0031-8949/23/5A/020.
80. A. Tauheed and A. Naz. J. Korean Phys. Soc. **59**, 2910 (2011). doi:10.3938/jkps.59.2910.
81. C.R. Cowley, T.R. Ayres, F. Castelli, A.F. Gulliver, R. Monier, and G.M. Wahlgren. Astrophys. J. **826**, 158 (2016). doi:10.3847/0004-637X/826/2/158.
82. W. Zhang, P. Palmeri, P. Quinet, É. Biémont, S. Du, and Z. Dai. Phys. Rev. A, **82**, 042507 (2010). doi:10.1103/PhysRevA.82.042507.
83. G. Malcheva, S. Enzonga, R. Mayo Yoca, M. Ortiz, L. Engström, H. Lundberg, H. Nilsson, É. Biémont, and K. Blagoev. Mon. Not. R. Astron. Soc. **396**, 2289 (2009). doi:10.1111/j.1365-2966.2009.14894.x.
84. V. Fivet, P. Palmeri, P. Quinet, É. Biémont, H.L. Xu, and S. Svanberg. Eur. Phys. J. D, **37**, 29 (2006). doi:10.1140/epjd/e2005-00256-8.
85. P. Quinet, V. Fivet, P. Palmeri, E. Biémont, L, H. Engström, H. Lundberg, and Nilsson. Astron. Astrophys. **493**, 711 (2009). doi:10.1051/0004-6361:200811035.
86. V. Fivet, É. Biémont, L. Engström, H. Lundberg, H. Nilsson, P. Palmeri, and P. Quinet. J. Phys. B: Atom. Mol. Opt. Phys. **41**, 015702 (2008). doi:10.1088/0953-4075/41/1/015702.
87. P. Palmeri, P. Quinet, É. Biémont, S. Svanberg, and H.L. Xu. Phys. Scr. **74**, 297 (2006). doi:10.1088/0031-8949/74/3/001.
88. P. Palmeri, P. Quinet, É. Biémont, H.L. Xu, and S. Svanberg. Mon. Not. R. Astr. Soc. **362**, 1348 (2005). doi:10.1111/j.1365-2966.2005.09408.x.
89. P. Quinet, P. Palmeri, E. Biémont, A. Jorissen, S. Van Eck, S. Svanberg, H.L. Xu, and B. Plez. Astron. Astrophys. **448**, 1207 (2006). doi:10.1051/0004-6361:20053852.
90. H.L. Xu, S. Svanberg, P. Quinet, P. Palmeri, and E. Biémont. J. Quant. Spectrosc. Radiat. Transfer, **104**, 52 (2007). doi:10.1016/j.jqsrt.2006.08.010.
91. P. Quinet, P. Palmeri, V. Fivet, É. Biémont, H. Nilsson, L. Engström, and H. Lundberg. Phys. Rev. A, **77**, 022501 (2008). doi:10.1103/PhysRevA.77.022501.
92. V. Fivet, P. Quinet, É. Biémont, and H.L. Xu. J. Phys. B: Atom. Mol. Opt. Phys. **39**, 3587 (2006). doi:10.1088/0953-4075/39/17/015.
93. M. Ortiz, R. Mayo, E. Biémont, P. Quinet, V. Fivet, G. Malcheva, and K. Blagoev. *In* 14th International School on Quantum Electronics: Laser Physics and Applications. *Edited by* P.A. Atanasov, T.N. Dreischuh, S.V. Gateva, L.M. Kovachev. Proceedings of SPIE, **6604**, 66040N (2007).
94. S.E. Yoca, É. Biémont, F. Delahaye, P. Quinet, and C.J. Zeippen. Phys. Scr. **78**, 025303 (2008). doi:10.1088/0031-8949/78/02/025303.
95. K. Blagoev, V. Pentchev, E. Biémont, Z.G. Zhang, C.-G. Wahlström, and S. Svanberg. Phys. Rev. A, **66**, 032509 (2002). doi:10.1103/PhysRevA.66.032509.
96. É. Biémont, P. Palmeri, P. Quinet, Z. Dai, S. Svanberg, and H.L. Xu. J. Phys. B: Atom. Mol. Opt. Phys. **38**, 3547 (2005). doi:10.1088/0953-4075/38/19/007.
97. Z.S. Li, S. Svanberg, E. Biémont, P. Palmeri, and J. Zhankui. Phys. Rev. A, **57**, 3443 (1998). doi:10.1103/PhysRevA.57.3443.
98. E. Biémont, H.-P. Garnir, P. Palmeri, Z.S. Li, and S. Svanberg. Mon. Not. R. Astron. Soc. **312**, 116 (2000). doi:10.1046/j.1365-8711.2000.03094.x.
99. P. Quinet, E. Biémont, P. Palmeri, and H.L. Xu. J. Phys. B: Atom. Mol. Opt. Phys. **40**, 1705 (2007). doi:10.1088/0953-4075/40/10/005.
100. P. Palmeri, P. Quinet, and E. Biémont. Phys. Scr. **63**, 468 (2001). doi:10.1238/Physica.Regular.063a00468.

101. M. Lundqvist, H. Nilsson, G.M. Wahlgren, H. Lundberg, H.L. Xu, Z.K. Jiang, et al. Astron. Astrophys. **450**, 407 (2006). doi:10.1051/0004-6361:20054474.
102. J.E. Lawler, E.A. Den Hartog, Z.E. Labby, C. Sneden, J.J. Cowan, and I.I. Ivans. Astrophys. J. Suppl. Ser. **169**, 120 (2007). doi:10.1086/510368.
103. S. Bouazza, P. Quinet, and P. Palmeri. J. Quant. Spectrosc. Rad. Transf. **163**, 39 (2015). doi:10.1016/j.jqsrt.2015.04.013.
104. P. Quinet, V. Vinogradoff, P. Palmeri, and E. Biémont. J. Phys. B: Atom. Mol. Opt. Phys. **43**, 144003 (2010). doi:10.1088/0953-4075/43/14/144003.
105. P. Quinet, P. Palmeri, and É. Biémont. J. Phys. B: Atom. Mol. Opt. Phys. **44**, 145005 (2011). doi:10.1088/0953-4075/44/14/145005.
106. H. Nilsson, L. Engström, H. Lundberg, P. Palmeri, V. Fivet, P. Quinet, and É. Biémont. Eur. Phys. J. D, **49**, 13 (2008). doi:10.1140/epjd/e2008-00131-2.
107. P. Palmeri, P. Quinet, V. Fivet, É. Biémont, H. Nilsson, L. Engström, and H. Lundberg. Phys. Scr. **78**, 015304 (2008). doi:10.1088/0031-8949/78/01/015304.
108. S.E. Yoca, P. Quinet, and É. Biémont. J. Phys. B: Atom. Mol. Opt. Phys. **45**, 035001 (2012). doi:10.1088/0953-4075/45/3/035001.
109. S.E. Yoca, P. Quinet, P. Palmeri, and É. Biémont. J. Phys. B: Atom. Mol. Opt. Phys. **45**, 065001 (2012). doi:10.1088/0953-4075/45/6/065001.
110. S.E. Yoca, P. Palmeri, P. Quinet, G. Jumet, and É. Biémont. J. Phys. B: At. Mol. Opt. Phys. **45**, 035002 (2012). doi:10.1088/0953-4075/45/3/035002.
111. J. Deprince and P. Quinet. Atoms, **3**, 299 (2015). doi:10.3390/atoms3030299.
112. A. Kramida and T. Shirai. Atom. Data Nucl. Data Tables, **95**, 305 (2009). doi:10.1016/j.adt.2008.12.002.
113. A.N. Ryabtsev, E.Y. Kononov, R.R. Kildiyarova, W.-Ü.L. Tchang-Brillet, and J.-F. Wyart. Phys. Scr. **87**, 045303 (2013). doi:10.1088/0031-8949/87/04/045303.
114. M.F. Gu. Astrophys. J. **582**, 1241 (2003). doi:10.1086/344745.
115. P. Quinet. J. Quant. Spectrosc. Rad. Transfer, **145**, 153 (2014). doi:10.1016/j.jqsrt.2014.05.003.
116. G.W. Charles. J. Opt. Soc. Am. **56**, 1292 (1966). doi:10.1364/JOSA.56.001292.
117. A. Kramida, Yu. Ralchenko, J. Reader, and NIST ASD Team. NIST Atomic Spectra Database, Gaithersburg, MD (2013).
118. T.E. Cocolios, B.A. Marsh, V.N. Fedosseev, et al. Nucl. Instrum. Meth. Phys. Res. B: Interact. Mater. Atoms, **266**, 4403 (2008). doi:10.1016/j.nimb.2008.05.142.
119. V.F. Gopka, A.V. Yushchenko, A.V. Shavrina, D.E. Mkrtichian, A.P. Hatzes, S.M. Andrievsky, et al. The A-Star Puzzle, Proc. of IAU Symposium, **224**, 734 (2004).
120. P. Palmeri, P. Quinet, and S. Bouazza. J. Quant. Spectrosc. Radiat. Transfer, **185**, 70 (2016). doi:10.1016/j.jqsrt.2016.08.014.
121. S. Kröger, G. Başar, A. Baier, and G.H. Guthörlein. Phys. Scr. **65**, 56 (2002). doi:10.1238/Physica.Regular.065a00056.
122. J.-F. Wyart. Phys. Scr. **82**, 035302 (2010). doi:10.1088/0031-8949/82/03/035302.
123. J.-F. Wyart. Can. J. Phys. **89**, 451 (2011). doi:10.1139/p10-112.
124. J.-F. Wyart and J.E. Lawler. Phys. Scr. **79**, 045301 (2009). doi:10.1088/0031-8949/79/04/045301.
125. E. Biémont, P. Quinet, S. Svanberg, and H.L. Xu. Eur. Phys. J. D, **30**, 157 (2004). doi:10.1140/epjd/e2004-00077-3.
126. E. Biémont, Z.S. Li, P. Palmeri, and P. Quinet. J. Phys. B: Atom. Mol. Opt. Phys. **32**, 3409 (1999). doi:10.1088/0953-4075/32/14/311.
127. P. Palmeri, P. Quinet, J.-F. Wyart, and E. Biémont. Phys. Scr. **61**, 323 (2000). doi:10.1238/Physica.Regular.061a00323.
128. Z.G. Zhang, S. Svanberg, Z. Jiang, P. Palmeri, P. Quinet, and E. Biémont. Phys. Scr. **63**, 122 (2001). doi:10.1238/Physica.Regular.063a00122.
129. E. Biémont, P. Quinet, S. Svanberg, and H.L. Xu. J. Phys. B: Atom. Mol. Opt. Phys. **37**, 1381 (2004). doi:10.1088/0953-4075/37/7/001.
130. E. Biémont, P.H. Lefebvre, P. Quinet, S. Svanberg, and H. Xu. Eur. Phys. J. D, **27**, 33 (2003). doi:10.1140/epjc/s2002-01087-0.
131. P. Palmeri, P. Quinet, Y. Frémat, J.-F. Wyart, and E. Biémont. Astrophys. J. Suppl. Ser. **129**, 367 (2000). doi:10.1086/313405.
132. E. Biémont, H.P. Garnir, P. Palmeri, P. Quinet, Z.S. Li, Z.G. Zhang, and S. Svanberg. Phys. Rev. A, **64**, 022503 (2001). doi:10.1103/PhysRevA.64.022503.
133. H. Xu, S. Svanberg, R.D. Cowan, P.H. Lefebvre, P. Quinet, and E. Biémont. Mon. Not. R. Astron. Soc. **346**, 433 (2003). doi:10.1046/j.1365-2966.2003.07107.x.
134. E. Biémont, A. Ellmann, P. Lundin, S. Mannervik, L.-O. Norlin, P. Palmeri, P. Quinet, D. Rostohar, P. Royen, and P. Schef. Eur. Phys. J. D, **41**, 211 (2007). doi:10.1140/epjd/e2006-00229-5.
135. Z.G. Zhang, S. Svanberg, P. Palmeri, P. Quinet, and E. Biémont. Astron. Astrophys. **385**, 724 (2002). doi:10.1051/0004-6361:20020148.
136. V. Fivet, P. Quinet, E. Biémont, A. Jorissen, A.V. Yushchenko, and S. Van Eck. Mon. Not. R. Astr. Soc. **380**, 771 (2007). doi:10.1111/j.1365-2966.2007.12118.x.
137. V. Fivet, P. Quinet, E. Biémont, A. Jorissen, A.V. Yushchenko, and S. Van Eck. Mon. Not. R. Astron. Soc. **382**, 944 (2007). doi:10.1111/j.1365-2966.2007.12453.x.
138. H. Xu, S. Svanberg, P. Quinet, H.P. Garnir, and E. Biémont. J. Phys. B: At. Mol. Opt. Phys. **36**, 4773 (2003). doi:10.1088/0953-4075/36/24/002.
139. E. Biémont, H.P. Garnir, U. Litzén, K. Nielsen, P. Quinet, S. Svanberg, G. Wahlgren, and Z.G. Zhang. Astron. Astrophys. **399**, 343 (2003). doi:10.1051/0004-6361:20021797.
140. P. Quinet and E. Biémont. Mon. Not. R. Astron. Soc. **340**, 463 (2003). doi:10.1046/j.1365-8711.2003.06319.x.
141. E. Biémont, G. Kohnen, and P. Quinet. Astron. Astrophys. **393**, 717 (2002). doi:10.1051/0004-6361:20021055.
142. E. Biémont, H.P. Garnir, P. Quinet, S. Svanberg, and Z.G. Zhang. Phys. Rev. A, **65**, 052502 (2002). doi:10.1103/PhysRevA.65.052502.
143. Z.G. Zhang, S. Svanberg, P. Palmeri, P. Quinet, and E. Biémont. Mon. Not. R. Astron. Soc. **334**, 1 (2002). doi:10.1046/j.1365-8711.2002.05259.x.
144. E. Biémont, P. Palmeri, P. Quinet, G. Paquin, Z.G. Zhang, G. Somesfalean, and S. Svanberg. Mon. Not. R. Astron. Soc. **328**, 1085 (2001). doi:10.1046/j.1365-8711.2001.04922.x.
145. Z.G. Zhang, G. Somesfalean, S. Svanberg, P. Palmeri, P. Quinet, and E. Biémont. Astron. Astrophys. **384**, 364 (2002). doi:10.1051/0004-6361:20020014.
146. H. Xu, Zhankui Jiang, Z.G. Zhang, Z. Dai, S. Svanberg, P. Quinet, and E. Biémont. J. Phys. B: Atom. Mol. Opt. Phys. **36**, 1771 (2003). doi:10.1088/0953-4075/36/9/309.
147. E. Biémont, H.P. Garnir, T. Bastin, P. Palmeri, P. Quinet, Z.S. Li, Z.G. Zhang, V. Lokhnygin, and S. Svanberg. Mon. Not. R. Astron. Soc. **321**, 481 (2001). doi:10.1046/j.1365-8711.2001.04032.x.
148. P. Quinet, P. Palmeri, and E. Biémont. J. Quant. Spectrosc. Rad. Transfer, **62**, 625 (1999). doi:10.1016/S0022-4073(98)00127-7.
149. Z.S. Li, Z.G. Zhang, V. Lokhnygin, S. Svanberg, T. Bastin, E. Biémont, H.P. Garnir, P. Palmeri, and P. Quinet. J. Phys. B: Atom. Mol. Opt. Phys. **34**, 1349 (2001). doi:10.1088/0953-4075/34/8/301.
150. E. Biémont and P. Quinet. Phys. Rev. Lett. **81**, 3345 (1998). doi:10.1103/PhysRevLett.81.3345.
151. E. Biémont, J.-F. Dutrieux, I. Martin, and P. Quinet. J. Phys. B: Atom. Mol. Opt. Phys. **31**, 3321 (1998). doi:10.1088/0953-4075/31/15/006.
152. Z.S. Li, S. Svanberg, P. Quinet, X. Tordoir, and E. Biémont. J. Phys. B: Atom. Mol. Opt. Phys. **32**, 1731 (1999). doi:10.1088/0953-4075/32/7/014.
153. E. Biémont, P. Quinet, Z. Dai, Jiang Zhankui, Z.G. Zhang, H. Xu, and S. Svanberg. J. Phys. B: Atom. Mol. Opt. Phys. **35**, 4743 (2002). doi:10.1088/0953-4075/35/22/315.
154. E. Biémont, H.P. Garnir, Z.S. Li, V. Lokhnygin, P. Palmeri, P. Quinet, S. Svanberg, J.F. Wyart, and Z.G. Zhang. J. Phys. B: Atom. Mol. Opt. Phys. **34**, 1869 (2001). doi:10.1088/0953-4075/34/10/302.
155. Z.G. Zhang, Z.S. Li, S. Svanberg, P. Palmeri, P. Quinet, and E. Biémont. Eur. Phys. J. D, **15**, 301 (2001). doi:10.1007/s100530170144.
156. J.A. Fedchak, E.A. Den Hartog, J.E. Lawler, P. Palmeri, P. Quinet, and E. Biémont. Astrophys. J. **542**, 1109 (2000). doi:10.1086/317034.
157. Z. Dai, Jiang Zhankui, H. Xu, Z.G. Zhang, S. Svanberg, E. Biémont, P.H. Lefèbvre, and P. Quinet. J. Phys. B: Atom. Mol. Opt. Phys. **36**, 479 (2003). doi:10.1088/0953-4075/36/3/306.
158. P. Quinet, P. Palmeri, E. Biémont, M.M. McCurdy, G. Rieger, E.H. Pinnington, M.E. Wickliffe, and J.E. Lawler. Mon. Not. R. Astr. Soc. **307**, 934 (1999). doi:10.1046/j.1365-8711.1999.02689.x.
159. Z.G. Zhang, S. Svanberg, P. Quinet, P. Palmeri, and E. Biémont. Phys. Rev. Lett. **87**, 273001 (2001). doi:10.1103/PhysRevLett.87.273001. PMID:11800875.
160. J.F. Wyart, W.U.L. Tchang-Brillet, N. Spector, P. Palmeri, P. Quinet, and E. Biémont. Phys. Scr. **63**, 113 (2001). doi:10.1238/Physica.Regular.063a00113.
161. S.E. Yoca and P. Quinet. J. Phys. B: Atom. Mol. Opt. Phys. **46**, 145003 (2013). doi:10.1088/0953-4075/46/14/145003.
162. S.E. Yoca and P. Quinet. J. Phys. B: Atom. Mol. Opt. Phys. **47**, 035002 (2014). doi:10.1088/0953-4075/47/3/035002.
163. E. Biémont, P. Quinet, and T.A. Ryabchikova. Mon. Not. R. Astron. Soc. **336**, 1155 (2002). doi:10.1046/j.1365-8711.2002.05868.x.
164. J.F. Wyart, A. Meftah, W.-Ü.L. Tchang-Brillet, N. Champion, O. Lamrous, N. Spector, and J. Sugar. J. Phys. B: Atom. Mol. Opt. Phys. **40**, 3957 (2007). doi:10.1088/0953-4075/40/19/013.
165. E. Biémont, P. Quinet, and V. Van Renterghem. J. Phys. B: Atom. Mol. Opt. Phys. **31**, 5301 (1998). doi:10.1088/0953-4075/31/24/012.
166. E. Peik and C. Tamm. Europhys. Lett. **61**, 181 (2003). doi:10.1209/epl/i2003-00210-x.
167. E. Biémont, V. Fivet, and P. Quinet. J. Phys. B: Atom. Mol. Opt. Phys. **37**, 4193 (2004). doi:10.1088/0953-4075/37/20/013.
168. W.P. Bidelman. ASP Conf. Ser. **336**, 309 (2005).
169. V.F. Gopka, A.V. Yushchenko, S. Goriely, A.V. Shavrina, and Y.W. Kang. AIP Conf. Proc. **847**, 389 (2006). doi:10.1063/1.2234435.
170. S. Goriely and M. Arnould. Astron. Astrophys. **379**, 1113 (2001). doi:10.1051/0004-6361:20011368.
171. V.F. Gopka, A.V. Yushchenko, A.V. Shavrina, D.E. Mkrtichian, A.P. Hatzes, S.M. Andrievsky, et al., Proc. Int. Symp. Nucl. Astrophys. – Nuclei in the Cosmos, CERN (2006).
172. A.V. Yushchenko, V.F. Gopka, S. Goriely, D. Lambert, A.V. Shavrina, Y.W. Kang, et al. ASP Conf. Ser. **362**, 46 (2007).
173. S. Goriely. Astron. Astrophys. **466**, 619 (2007). doi:10.1051/0004-6361:20066583.
174. P. Quinet, C. Argante, V. Fivet, C. Terranova, A.V. Yushchenko, and É. Biémont. Astron. Astrophys. **474**, 307 (2007). doi:10.1051/0004-6361:20078082.
175. V. Fivet, P. Quinet, and E. Biémont. J. Elect. Spectrosc. Rel. Phenom. **156–158**, 255 (2007).
176. Th. Arndt, H. Backe, A. Steinhof, P. Dyer, M.M. Fowler, P.G. Eller, and J.B. Wihelmy. Phys. Rev. A, **38**, 5084 (1988). doi:10.1103/PhysRevA.38.5084.
177. E. Biémont, P. Palmeri, P. Quinet, Z.G. Zhang, and S. Svanberg. Astrophys. J. **567**, 1276 (2002). doi:10.1086/338700.
178. E. Biémont, P. Palmeri, P. Quinet, S. Svanberg, and Z.G. Zhang. J. Phys. B: Atom. Mol. Opt. Phys. **35**, 1701 (2002). doi:10.1088/0953-4075/35/7/308.

179. T. Ryabchikova, M. Sachkov, W.W. Weiss, et al. Astron. Astrophys. **462**, 1103 (2007). doi:10.1051/0004-6361:20066365.
180. K. Werner, T. Rauch, E. Ringat, and J.W. Kruk. Astrophys. J. **753**, L7 (2012). doi:10.1088/2041-8205/753/1/L7.
181. T. Rauch, S. Gamrath, P. Quinet, L. Löbling, D. Hoyer, K. Werner, J.W. Kruk and M. Demleitner. Astron. Astrophys. Forthcoming article. (2016). doi:10.1051/0004-6361/201629794.
182. T. Rauch, P. Quinet, D. Hoyer, K. Werner, M. Demleitner, and J.W. Kruk. Astron. Astrophys. **587**, A39 (2016). doi:10.1051/0004-6361/201527324.
183. T. Rauch, D. Hoyer, P. Quinet, M. Gallardo, and M. Raineri. Astron. Astrophys. **577**, A88 (2015). doi:10.1051/0004-6361/201526078.
184. T. Rauch, K. Werner, P. Quinet, and J.W. Kruk. Astron. Astrophys. **566**, A10 (2014). doi:10.1051/0004-6361/201423878.
185. T. Rauch, K. Werner, P. Quinet, and J.W. Kruk. Astron. Astrophys. **564**, A41 (2014). doi:10.1051/0004-6361/201423491.
186. T. Rauch, K. Werner, P. Quinet, and W. Kruk. Astron. Astrophys. **577**, A6 (2015). doi:10.1051/0004-6361/201425326.
187. T. Rauch, K. Werner, É. Biémont, P. Quinet, and J.W. Kruk. Astron. Astrophys. **546**, A55 (2012). doi:10.1051/0004-6361/201220014.
188. T. Rauch, P. Quinet, D. Hoyer, K Werner, P. Richter, J.W. Kruk, and M. Demleitner. Astron. Astrophys. **590**, A128 (2016). doi:10.1051/0004-6361/201628131.
189. E. Biémont, P. Palmeri, and P. Quinet. Astrophys. Space Sci. **269–270**, 635 (1999). doi:10.1007/978-94-011-4114-7_64.
190. E. Biémont and P. Quinet. J. Electr. Spectrosc. Rel. Phen. **144–147**, 23 (2005).
191. V. Fivet, P. Quinet, P. Palmeri, E. Biémont, and H.L. Xu. J. Elec. Spectrosc. Rel. Phen. **156–158**, 250 (2007).
192. M.L. Dubernet, B.K. Antony, Y.A. Ba, et al. J. Phys. B: Atom. Mol. Opt. Phys. **49**, 074003 (2016). doi:10.1088/0953-4075/49/7/074003.